NASA CONTRACTOR REPORT

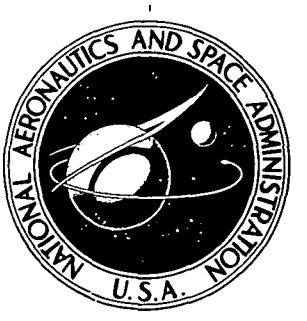

NASA CR-2285

NASA CR-2285

SOME PROBLEMS OF THE CALCULATION OF THREE-DIMENSIONAL BOUNDARY-LAYER FLOWS ON GENERAL CONFIGURATIONS

by Tuncer Cebeci, Kalle Kaups, G. J. Mosinskis, and J. A. Rehn

Prepared by
DOUGLAS AIRCRAFT COMPANY
MCDONNELL DOUGLAS CORPORATION
Long Beach, Calif. 90801
for Langley Research Center

NATIONAL AERONAUTICS AND SPACE ADMINISTRATION • WASHINGTON, D. C. • JULY 1973

1. Report No.	2. Government Accession No.	3. Recipient's Catalog No.
NASA CR-2285		

4. Title and Subtitle	5. Report Date
SOME PROBLEMS OF THE CALCULATION OF THREE-DIMENSIONAL BOUNDARY-LAYER FLOWS ON GENERAL CONFIGURATIONS	July 1973
	6. Performing Organization Code

7. Author(s)	8. Performing Organization Report No.
Tuncer Cebeci, Kalle Kaups, G. J. Mosinskis, and J. A. Rehn	
	10. Work Unit No.

9. Performing Organization Name and Address	11. Contract or Grant No.
McDonnell Douglas Corporation Long Beach, CA 90801	NAS 1-11623
	13. Type of Report and Period Covered
12. Sponsoring Agency Name and Address	Contractor Report
	14. Sponsoring Agency Code

15. Supplementary Notes

16. Abstract

An accurate solution of the three-dimensional boundary-layer equations over general configurations such as those encountered in aircraft and space shuttle design requires a very efficient, fast, and accurate numerical method with suitable turbulence models for the Reynolds stresses. This study investigates the efficiency, speed, and accuracy of a three-dimensional numerical method together with the turbulence models for the Reynolds stresses. The numerical method is the implicit two-point finite-difference approach (Box Method) developed by H. B. Keller and applied to the boundary-layer equations by Keller and Cebeci. In addition, report presents a study of some of the problems that may arise in the solution of these equations for three-dimensional boundary layer flows over general configurations.

17. Key Words (Suggested by Author(s))	18. Distribution Statement
Three-dimensional boundary layer Turbulent flow Three-dimensional flow Computational fluid dynamics	Unclassified - Unlimited

19. Security Classif. (of this report)	20. Security Classif. (of this page)	21. No. of Pages	22. Price*
Unclassified	Unclassified	56	$3.00

*For sale by the National Technical Information Service, Springfield, Virginia 22151

Page Intentionally Left Blank

TABLE OF CONTENTS

LIST OF SYMBOLS

A	Van Driest damping parameter
c_f	local skin-friction coefficient, $\tau_w/(1/2)\rho_e u_e^2$
c_p	specific heat at constant pressure
C	viscosity-density parameter
C^*	a Reynolds number eq. (4.3.1)
f	similarity variable for ψ
g	similarity variable for ϕ
h_1, h_2	metric coefficients
H	total enthalpy
J	total number of grid points in η-direction
K	variable grid parameter
K_1, K_2	geodesic curvatures
L	modified mixing length
M	Mach number, wherever applicable
p	pressure
p^+	dimensionless pressure gradient parameter
Pr	Prandtl number, $\mu c_p/\lambda_\ell$
Pr_t	turbulent Prandtl number, $\varepsilon^+/\varepsilon_\theta^+$
R_s, R_x	Reynolds number, $u_s x/\nu$ and $u_e x/\nu$, respectively
R_θ	Reynolds number, $u_s \theta/\nu$
u, v, w	velocity components in the x,y,z-directions, respectively
u_τ	friction velocity
w_z	derivative of w with respect to z, $\partial w/\partial z$
x	surface coordinate or streamline coordinate
y	coordinate normal to the body surface
z	surface coordinate normal to the x-coordinate
α	parameter in the outer eddy-viscosity formula, or angle with x-axis, wherever applicable
γ	intermittency factor, or inviscid flow direction, wherever applicable
δ	boundary layer thickness
$\varepsilon, \varepsilon_\theta$	eddy viscosity and eddy conductivity, respectively
$\varepsilon^+, \varepsilon_\theta^+$	dimensionless eddy viscosity, ε/ν and eddy conductivity, ε_θ/ν

η similarity variable for y

η_∞ transformed boundary-layer thickness

θ momentum thickness $\int_0^\infty u/u_s\,(1 - u/u_s)dy$ or total enthalpy ratio, H/H_e wherever applicable

κ von Karman's constant

λ_ℓ thermal conductivity

μ dynamic viscosity

ν kinematic viscosity

ξ similarity variable for x

ρ density

τ shear stress

ϕ,ψ components of vector potential

Subscripts

e outer edge of boundary layer

s direction of inviscid streamlines

tr transition

w wall

x,z x- and z-components, respectively

o reference conditions

∞ freestream conditions

Primes denote differentiation with respect to η

SOME PROBLEMS OF THE CALCULATION OF THREE-DIMENSIONAL BOUNDARY-LAYER FLOWS ON GENERAL CONFIGURATIONS

by

Tuncer Cebeci, Kalle Kaups, G. J. Mosinskis, J. A. Rehn
Douglas Aircraft Company

I. SUMMARY

An accurate solution of the three-dimensional boundary-layer equations over general configurations such as those encountered in aircraft and space shuttle design requires a very efficient, fast, and accurate numerical method with suitable turbulence models for the Reynolds stresses. In the study reported here, we investigate the efficiency, speed, and accuracy of a numerical method together with the turbulence models for the Reynolds stresses. The numerical method is an implicit two-point finite-difference method (Box Method) developed by H. B. Keller (ref. 1) and applied to the boundary-layer equations by Keller and Cebeci (refs. 2, 3). In addition, we study some of the problems that may arise in the solution of these equations.

In Chapter II we write the governing boundary-layer equations, in both streamline and body coordinates, for three-dimensional, compressible, laminar and turbulent boundary layers. Those equations require initial conditions on two intersecting lines. Hence, we discuss the specifications of the initial conditions in longitudinal and lateral directions and the initial starting conditions, such as those existing in the nose region and those existing in the fuselage-wing junctures. We discuss the relative advantages of streamline and body coordinates and outline a solution procedure that combines both streamline and body coordinates.

When physical coordinates are used, the solutions of the governing boundary-layer equations are quite sensitive to the spacings in the streamwise direction (x), and the crosswise direction (z), and require a large number of x- and z-stations. In problems where computation time and storage become important, it is necessary to remove the sensitivity to Δx- and Δz-spacings. That can be done by expressing and by solving the governing equations in transformed coordinates. We, therefore, consider, in Chapter II, a convenient transformation and express the boundary-layer equations in terms of transformed variables.

In Chapter III we discuss Keller's Box Method. We investigate the computation time and the accuracy of the method for two-dimensional and three-dimensional flows, and we compare the stability properties of the Box Method with the stability properties of the method used by Krause, Hirschel, and Bothmann (ref. 4).

In Chapter IV we discuss and present a suitable turbulence model for three-dimensional compressible flows. The model, which is based on the concepts of eddy viscosity and eddy conductivity (turbulent Prandtl number), has given accurate results for two-dimensional incompressible and compressible flows and for three-dimensional incompressible flows. We also present results obtained with that formulation for an attachment-line, incompressible, turbulent flow on an infinite swept wing.

Finally, in Chapter V we outline a procedure for computing the compressible three-dimensional multi-component-gas boundary layers on general configurations. On the basis of the studies conducted in the earlier chapters, we estimate the computation time and computer-storage requirements.

II. GOVERNING EQUATIONS

2.1 The Boundary-Layer Equations in Streamline Coordinates

The governing boundary-layer equations for three-dimensional compressible flows in a curvilinear orthogonal coordinate system are given by the following equations:

Continuity

$$\frac{\partial}{\partial x}(\rho h_2 u) + \frac{\partial}{\partial z}(\rho h_1 w) + \frac{\partial}{\partial y}(h_1 h_2 \overline{\rho v}) = 0 \ , \qquad (2.1.1)$$

x-Momentum

$$\rho \frac{u}{h_1}\frac{\partial u}{\partial x} + \rho \frac{w}{h_2}\frac{\partial u}{\partial z} + \overline{\rho v}\frac{\partial u}{\partial y} - \rho u w K_2 + \rho w^2 K_1 = -\frac{1}{h_1}\frac{\partial p}{\partial x} + \frac{\partial}{\partial y}\left(\mu \frac{\partial u}{\partial y} - \rho \overline{u'v'}\right), \qquad (2.1.2)$$

z-Momentum

$$\rho \frac{u}{h_1}\frac{\partial w}{\partial x} + \rho \frac{w}{h_2}\frac{\partial w}{\partial z} + \overline{\rho v}\frac{\partial w}{\partial y} - \rho u w K_1 + \rho u^2 K_2 = -\frac{1}{h_2}\frac{\partial p}{\partial z} + \frac{\partial}{\partial y}\left(\mu \frac{\partial w}{\partial y} - \rho \overline{w'v'}\right), \qquad (2.1.3)$$

Energy

$$\rho \frac{u}{h_1}\frac{\partial H}{\partial x} + \rho \frac{w}{h_2}\frac{\partial H}{\partial z} + \overline{\rho v}\frac{\partial H}{\partial y} = \frac{\partial}{\partial y}\left[\frac{\mu}{Pr}\frac{\partial H}{\partial y} + \mu\left(1 - \frac{1}{Pr}\right)\frac{\partial}{\partial y}\left(\frac{u^2 + w^2}{2}\right) - \rho \overline{v'H'}\right], \qquad (2.1.4)$$

where $\overline{\rho v} = \rho v + \overline{\rho' v'}$ and h_1 and h_2 are metric coefficients. The latter are functions of x and z, that is,

$$h_1 = h_1(x,z), \qquad h_2 = h_2(x,z). \qquad (2.1.5a)$$

The parameters K_1 and K_2 are known as the geodesic curvatures of the curves x=const. and z=const., respectively. They are given by

$$K_1 = -\frac{1}{h_1 h_2}\frac{\partial h_2}{\partial x}, \qquad K_2 = -\frac{1}{h_1 h_2}\frac{\partial h_1}{\partial z}. \qquad (2.1.5b)$$

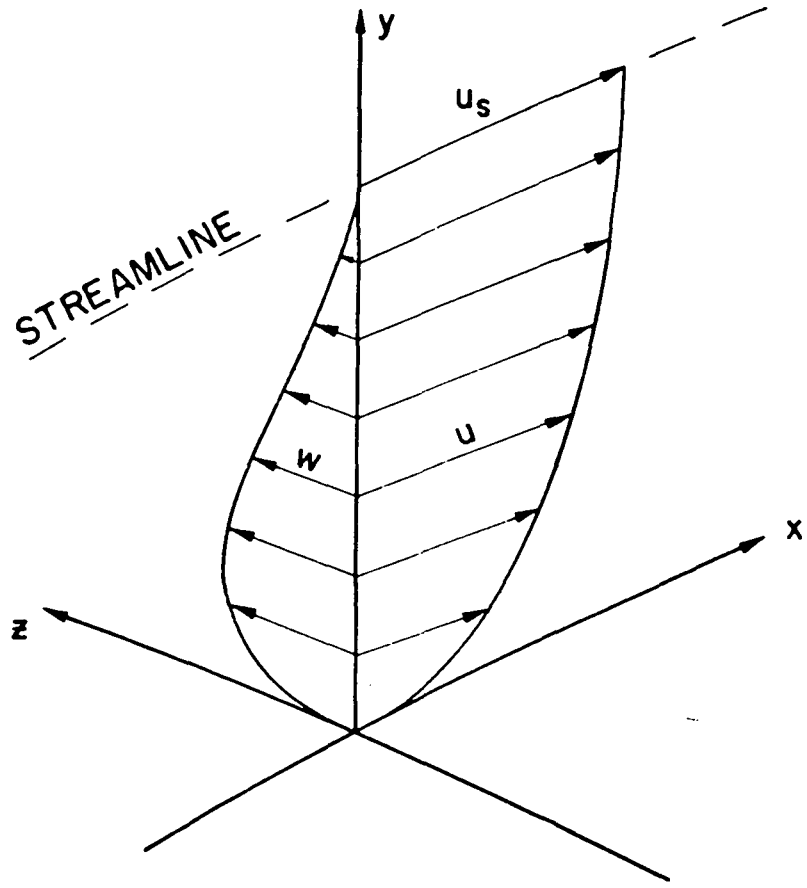

Figure 1. Streamline Coordinate System

The streamline coordinate system is also an orthogonal coordinate system formed by the inviscid streamlines and their orthogonal trajectories on the surface. As is shown in figure 1, the projection of the free-stream velocity vector on the surface is aligned with the surface coordinate x. The velocity component along the z-axis, referred to as the cross-flow velocity is zero at the edge of the boundary layer. The x-momentum equation (2.1.2) is referred to as the streamwise momentum, and the z-momentum equation is referred to as the cross-flow momentum equation.

At the edge of the boundary layer, (2.1.2) and (2.1.3) reduce to

$$\rho_s \frac{u_s}{h_1} \frac{\partial u_s}{\partial x} = -\frac{1}{h_1} \frac{\partial p}{\partial x} \qquad (2.1.6a)$$

$$\rho_s u_s^2 K_2 = -\frac{1}{h_2} \frac{\partial p}{\partial z} \qquad (2.1.6b)$$

The boundary conditions for the governing equations in streamline coordinates, (2.1.1) to (2.1.4), are

$$y = 0 \qquad u,w = 0, \qquad v = v_w(x,z)$$
$$H = H_w \quad \text{or} \quad \left(\frac{\partial H}{\partial y}\right)_w = H'_w \ \text{(given)} \tag{2.1.7a}$$

$$y = \delta \qquad u = u_s(x,z), \quad w = 0, \quad H = H_s \tag{2.1.7b}$$

The solution of the system given by (2.1.1) to (2.1.4) requires closure assumptions for the Reynolds stresses appearing in these equations. They also require initial conditions on two intersecting lines. In some problems the initial conditions can be established with ease; in some problems they require careful studies. As an example, consider the blunted circular cone with an elliptic cap shown in figure 2. It is clear that before the points B_2 and C_2 can be calculated, it is necessary to calculate the initial points A_1, A_2, B_1 and C_1.

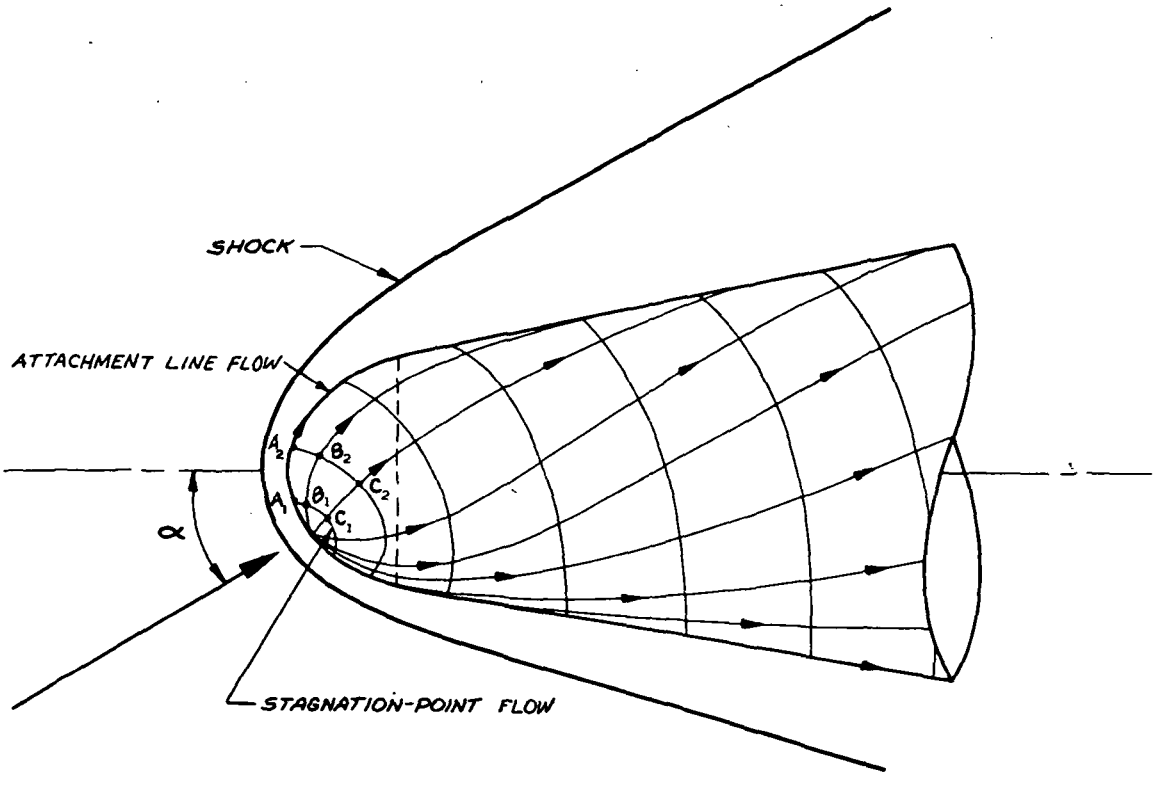

Figure 2. Blunted Circular Cone with Elliptic Nose Cap. Dashed Line Separates the Nose Cap from the Conical Configuration.

The initial points in the longitudinal direction, namely, A_1 and A_2 can be calculated by taking advantage of the symmetry conditions since in that direction the flow is two dimensional except for the cross-flow derivatives. The flow in that direction is usually referred to as the attachment-line flow, because the attachment line is a streamline on the body on which both the cross-flow velocity components in the boundary layer and the cross-flow pressure gradient are identically zero. Since w, K_2 are zero on the attachment line, the cross-flow momentum equation is singular on that line. However, differentiation with respect to z will yield a nonsingular equation. After performing the necessary differentiation for the cross-flow momentum equation and taking advantage of symmetry conditions, we can write the governing attachment-line flow equations as:

Continuity

$$\frac{\partial}{\partial x}(\rho h_2 u) + \rho h_1 w_z + \frac{\partial}{\partial y}(h_1 h_2 \overline{\rho v}) = 0 \tag{2.1.8}$$

Streamwise Momentum

$$\rho \frac{u}{h_1}\frac{\partial u}{\partial x} + \overline{\rho v}\frac{\partial u}{\partial y} = \rho_s \frac{u_s}{h_1}\frac{\partial u_s}{\partial x} + \frac{\partial}{\partial y}\left(\mu \frac{\partial u}{\partial y} - \rho\overline{u'v'}\right) \tag{2.1.9}$$

Cross-Flow Momentum

$$\rho \frac{u}{h_1}\frac{\partial w_z}{\partial x} + \frac{\rho}{h_2} w_z^2 + \overline{\rho v}\frac{\partial w_z}{\partial y} - \rho u K_1 w_z = \frac{\partial K_2}{\partial z}\rho_s u_s^2\left(1 - \frac{\rho u^2}{\rho_s u_s^2}\right) + \frac{\partial}{\partial y}\left[\mu \frac{\partial w_z}{\partial y} - \rho(\overline{w'v'})_z\right] \tag{2.1.10}$$

Energy

$$\rho \frac{u}{h_1}\frac{\partial H}{\partial x} + \overline{\rho v}\frac{\partial H}{\partial y} = \frac{\partial}{\partial y}\left[\frac{\mu}{Pr}\frac{\partial H}{\partial y} + \mu\left(1 - \frac{1}{Pr}\right)\frac{\partial}{\partial y}\left(\frac{u^2}{2}\right) - \rho\overline{v'H'}\right] \tag{2.1.11}$$

where $w_z = \partial w/\partial z$.

The attachment-line flow equations are subject to the following boundary conditions:

$$y = 0 \qquad u, w_z = 0 \qquad v = v_w(x,z)$$

$$H = H_w \quad \text{or} \quad \left(\frac{\partial H}{\partial y}\right)_w = H'_w \ \text{(given)} \tag{2.1.12a}$$

$$y = \delta \qquad u = u_s(x,z), \quad w_z = 0, \quad H = H_s \qquad (2.1.12b)$$

The initial points A_1 and A_2 can be obtained by solving the system (2.1.8) to (2.1.12). Again, however, the equations are singular at the first point (in our case A_1) and require starting conditions. These and the initial conditions in the lateral direction, namely, B_1, C_1, etc., can be obtained by constructing special solutions in the neighborhood of the stagnation point. At first, however, it is necessary to obtain the similarity equations known as the stagnation-point equations. They can be obtained by the procedure described below.

The governing conservation equations for three-dimensional laminar compressible flows in rectangular coordinates are

Continuity

$$\frac{\partial}{\partial x}(\rho u) + \frac{\partial}{\partial z}(\rho w) + \frac{\partial}{\partial y}(\rho v) = 0 \qquad (2.1.13)$$

x-Momentum

$$\rho u \frac{\partial u}{\partial x} + \rho w \frac{\partial u}{\partial z} + \rho v \frac{\partial u}{\partial y} = -\frac{\partial p}{\partial x} + \frac{\partial}{\partial y}\left(\mu \frac{\partial u}{\partial y}\right) \qquad (2.1.14)$$

z-Momentum

$$\rho u \frac{\partial w}{\partial x} + \rho w \frac{\partial w}{\partial z} + \rho v \frac{\partial w}{\partial y} = -\frac{\partial p}{\partial z} + \frac{\partial}{\partial y}\left(\mu \frac{\partial w}{\partial y}\right) \qquad (2.1.15)$$

Energy

$$\rho u \frac{\partial H}{\partial x} + \rho w \frac{\partial H}{\partial z} + \rho v \frac{\partial H}{\partial y} = \frac{\partial}{\partial y}\left[\frac{\mu}{Pr}\frac{\partial H}{\partial y} - \mu\left(1 - \frac{1}{Pr}\right)\frac{\partial}{\partial y}\left(\frac{u^2 + w^2}{2}\right)\right] \qquad (2.1.16)$$

We define a two-component vector potential by

$$\rho u = \frac{\partial \psi}{\partial y}, \qquad \rho w = \frac{\partial \phi}{\partial y}, \qquad \rho v = -\left(\frac{\partial \psi}{\partial x} + \frac{\partial \phi}{\partial z}\right) \qquad (2.1.17a)$$

and introduce the following transformation

$$d\xi = \rho_o \mu_o u_e dx, \qquad d\eta = \frac{\rho u_e}{(2\xi)^{1/2}} dy \qquad (2.1.17b)$$

together with two scalar functions ψ and ϕ defined by

$$\psi = (2\xi)^{1/2} f(\eta), \qquad \phi = (2\xi)^{1/2} \frac{w_e}{u_e} g(\eta) \tag{2.1.17c}$$

The subscript o denotes the reference conditions, and the subscript e denotes the edge conditions.

Introducing the relations given by (2.1.17) into (2.1.14) to (2.1.16), we get

$$(Cf'')' + \rho_e/\rho - (f')^2 + ff'' + cgf'' = 0 \tag{2.1.18}$$

$$(Cg'')' + c[\rho_e/\rho - (g')^2 + gg''] + fg'' = 0 \tag{2.1.19}$$

$$\left(\frac{C}{Pr}\theta'\right)' + (f + cg)\theta' = 0 \tag{2.1.20}$$

where the primes denote differentiation with respect to the similarity parameter η. Those equations assume that the outer flow is irrotational and that its components, upon suitable rotation of coordinates, are given by $u_e = Ax$ and $w_e = Bz$, where the constants A and B are related to the shape of the body near the stagnation point. In addition, the parameters C, c, f', g' and θ are defined by the following expressions:

$$C = \frac{\rho\mu}{\rho_o\mu_o}, \quad c = B/A, \quad f' = \frac{u}{u_e}, \quad g' = \frac{w}{w_e}, \quad \theta = H/H_e \tag{2.1.21}$$

The system given by (2.1.18) to (2.1.20) is subject to the following boundary conditions:

$$\eta = 0 \qquad f = f' = g = g' = 0, \qquad \theta = \theta_w \quad \text{or} \quad \theta_w' = \text{given} \tag{2.1.22a}$$

$$\eta = \eta_\infty \qquad f' = g' = 1 \qquad \theta = 1 \tag{2.1.22b}$$

Once the system (2.1.18) to (2.1.22) is solved, the initial conditions in the streamwise and the crosswise directions can be obtained in the following way.

Let us use x_o and z_o to denote the location at which we want to specify the profiles. The velocity profile making an angle α with the x-axis is

$$u = u_e f' \cos\alpha + w_e g' \sin\alpha$$

and the external flow component u_s is

$$u_s = u_e \cos \alpha + w_e \sin \alpha$$

Then the nondimensional streamwise profile is

$$\frac{u}{u_s} = \frac{f' + c(z_o/x_o)g' \tan \alpha}{1 + c\, z_o/x_o \tan \alpha}$$

If α is associated with the streamline direction (see figure 3), that expression becomes

$$\frac{u}{u_s} = \frac{f' + c^2(z_o/x_o)^2 g'}{1 + c^2(z_o/x_o)^2} \qquad (2.1.23)$$

Similarly, the cross-flow component w at the same location is

$$\frac{w}{u_s} = \frac{c\, z_o/x_o\, (g' - f')}{1 + c^2\, (z_o/x_o)^2} \qquad (2.1.24)$$

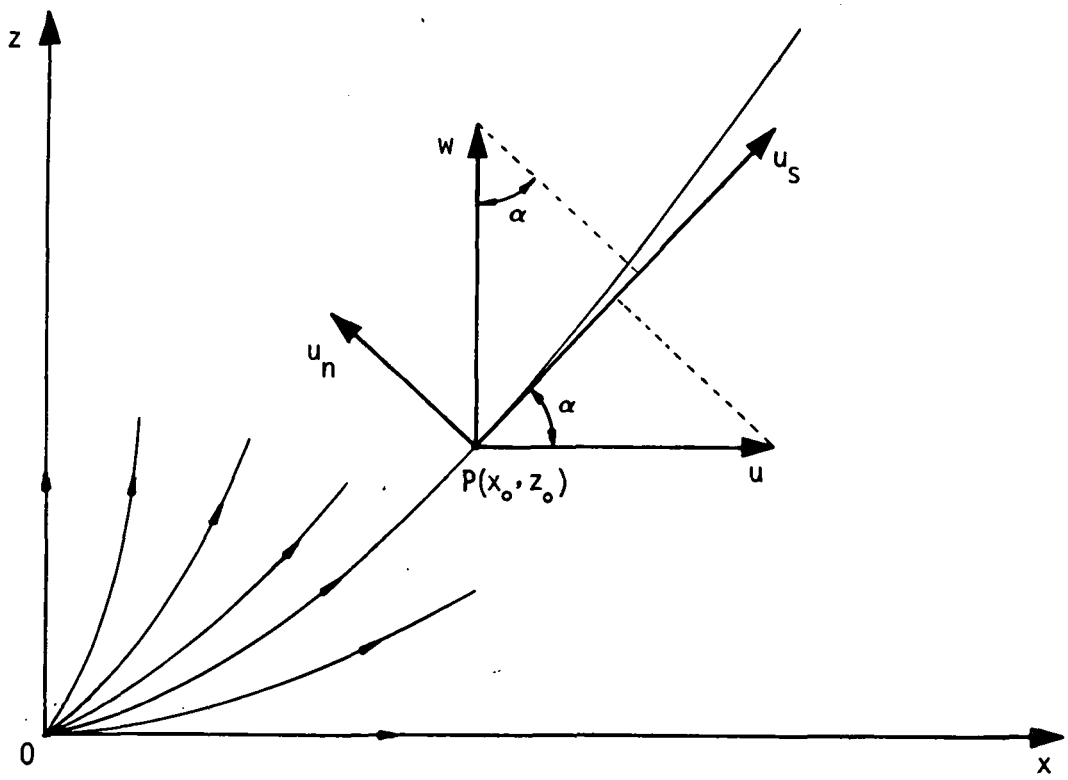

Figure 3. Resolution of the Velocity Profiles Near the Stagnation Point into Streamwise and Cross-Wise Components, $\tan \alpha = w_e/u_e = c\, z_o/x_o$.

The velocity profiles given by (2.1.23) and (2.1.24) can now be used as initial velocity profiles at B_1. They can also be used to represent the initial profiles at A_1 (note that $w \equiv 0$ now). However, better initial profiles in the neighborhood of the stagnation point can also be obtained by following the procedure discussed by Squire (ref. 5). Once the profiles at A_1 are known, the attachment-line flow equations (2.1.8) to (2.1.12) can be solved to obtain the solution at A_2. Then it is obvious that the general streamline equations (2.1.1) to (2.1.4) can be solved subject to the boundary conditions (2.1.7).

There are other practical problems in which the initial conditions as described in figure 1 cannot be obtained as readily. As an example, consider figure 4. Here, the initial conditions require special considerations. Clearly, the attachment line AB along the wing leading edge is a plane of

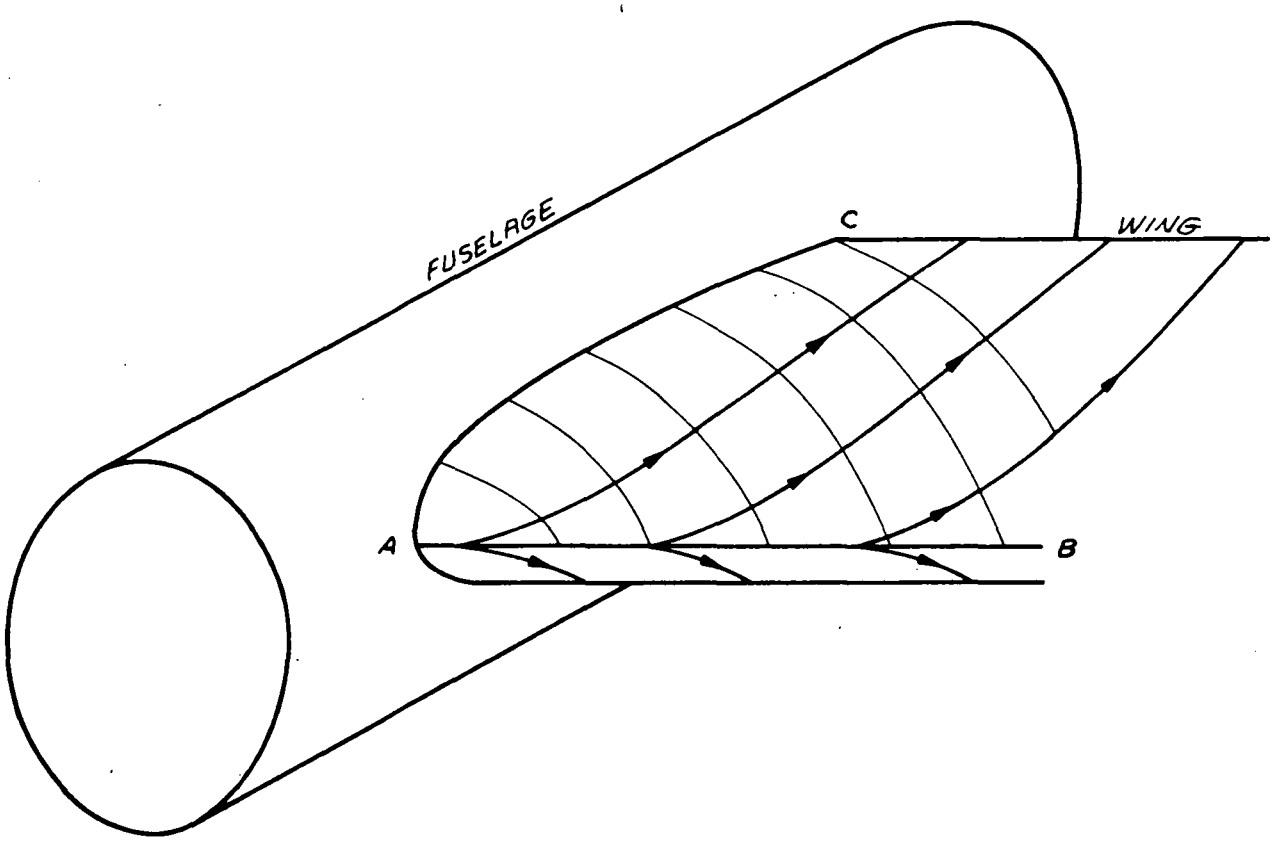

Figure 4. Fuselage-Wing Configuration

symmetry, and the initial conditions on AB can be calculated as before by solving the attachment-line flow equations. However, the initial conditions on AC that form the wing-fuselage juncture cannot be calculated easily. In fact, the viscous flow along the line AC is not of the boundary-layer type. It belongs to a class known as the boundary-region type. Certain approximations must be made to specify initial conditions on that line.

2.2 The Boundary-Layer Equations in Body Coordinates

2.2.1 Remarks on the Two Coordinate Systems

The discussion in Section 2.1 concerning figure 1 was based on the assumption that calculations from the initial data lines are to proceed in a streamline coordinate system. Although the streamline coordinate system is very general, its calculation is a major undertaking in itself and must be repeated at every change of attitude of the body. If the body is relatively simple, advantage can be taken of a geometry-oriented (body) coordinate system, which will eliminate the need to calculate the streamlines for each change of attitude or Mach number. The only disadvantage of body coordinates is that the initial lines cannot always be made to coincide with the body coordinate lines. For example, on a body of revolution (see fig. 5)

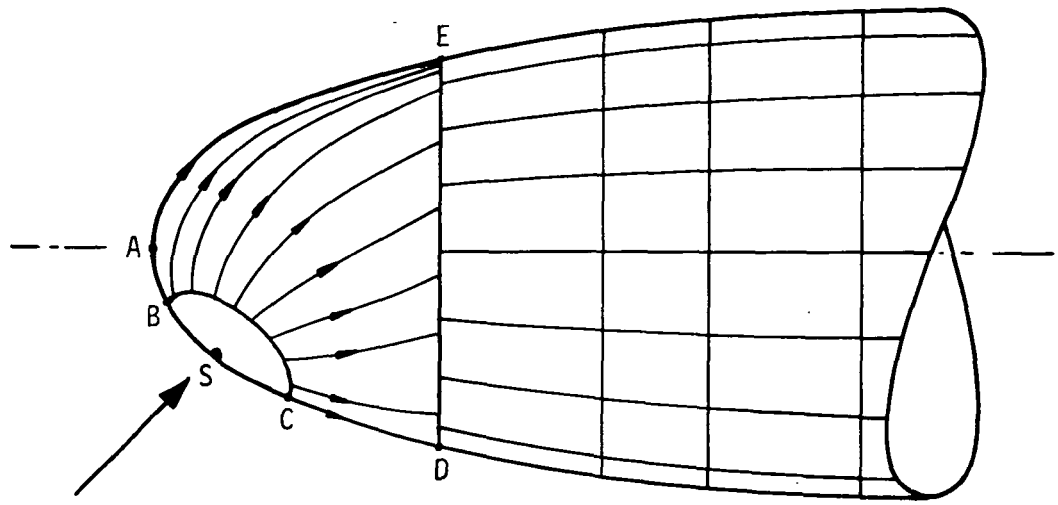

Figure 5. A Body of Revolution at an Angle of Attack

at an angle of attack, the stagnation point S is removed from the nose, which is the origin of the body-coordinate system. In order to start the solution, it is necessary to calculate the stagnation-point flow along the line BC. To proceed further, it is convenient to use streamline coordinates for a short distance in order to avoid the body singularity at A. The change from streamline coordinates to body coordinates should be done at a constant value of one body coordinate, for example, on line ED. The location of the line ED is arbitrary as long as point D is aft of point C. As shown in figure 5, the inviscid streamlines do not necessarily intersect the line ED at a constant body-coordinate interval. For that reason, interpolation of the rotated profiles (to be discussed in Section 2.2.2) on the line ED is unavoidable if calculations with constant increments in the body coordinates are desired.

2.2.2 Equations in Body Coordinates

The governing boundary-layer equations for three-dimensional compressible flows in body coordinates are given by (2.1.1) to (2.1.5).

At the edge of the boundary layer, (2.1.2) and (2.1.3) reduce to

$$\rho_e \frac{u_e}{h_1}\frac{\partial u_e}{\partial x} + \rho_e \frac{w_e}{h_2}\frac{\partial u_e}{\partial z} - \rho_e u_e w_e K_2 + \rho_e w_e^2 K_1 = -\frac{1}{h_1}\frac{\partial p}{\partial x} \qquad (2.2.1a)$$

$$\rho_e \frac{u_e}{h_1}\frac{\partial w_e}{\partial x} + \rho_e \frac{w_e}{h_2}\frac{\partial w_e}{\partial z} - \rho_e u_e w_e K_1 + \rho_e u_e^2 K_2 = -\frac{1}{h_2}\frac{\partial p}{\partial z} \qquad (2.2.1b)$$

The boundary conditions for the governing equations in body coordinates are

$y = 0$ $\qquad u, w = 0, \qquad v = v_w(x,z)$

$$H = H_w, \quad \text{or} \quad \left(\frac{\partial H}{\partial y}\right)_w = H'_w \quad \text{(given)} \qquad (2.2.2a)$$

$$y = \delta \qquad u = u_w(x,z), \quad w = w_e(x,z), \quad H = H_e \qquad (2.2.2b)$$

Making use of the symmetry conditions, we can write the two attachment-line flow momentum equations as

x-Momentum

$$\rho \frac{u}{h_1}\frac{\partial u}{\partial x} + \overline{\rho v}\frac{\partial u}{\partial y} = -\frac{1}{h_1}\frac{\partial p}{\partial x} + \frac{\partial}{\partial y}\left(\mu \frac{\partial u}{\partial y} - \rho\overline{u'v'}\right) \qquad (2.2.3)$$

z-Momentum

$$\rho \frac{u}{h_1} \frac{\partial w_z}{\partial x} + \rho \frac{1}{h_2} w_z^2 + \overline{\rho v} \frac{\partial w_z}{\partial y} - \rho u K_1 w_z + \rho u^2 \frac{\partial K_2}{\partial z}$$

$$= -\frac{1}{h_2} \frac{\partial^2 p}{\partial z^2} + \frac{\partial}{\partial y} \left[\mu \frac{\partial w_z}{\partial y} - \rho (\overline{w'v'})_z \right] \qquad (2.2.4)$$

The continuity and the energy equations are still the same, (2.1.8) and (2.1.11), respectively. Similarly, the boundary conditions are the same as (2.1.12), except that now the subscript s on u and H should be replaced by e.

The solution of the governing equations in body-coordinates aft of line ED (see fig. 5) requires initial velocity profiles, which come from the solution of the governing equations in the streamline coordinates. Except for the attachment line, they can be obtained in the following way.

Let us write the velocity components in streamline coordinates with bars, namely, $\bar{u}$, $\bar{w}$, and the angle the external streamline makes with the body coordinate x-direction as γ (see fig. 6). Then the velocity components u and w in the body-coordinate system x and z are

$$u = \bar{u} \cos \gamma - \bar{w} \sin \gamma \qquad (2.2.5a)$$

$$w = \bar{u} \sin \gamma + \bar{w} \cos \gamma \qquad (2.2.5b)$$

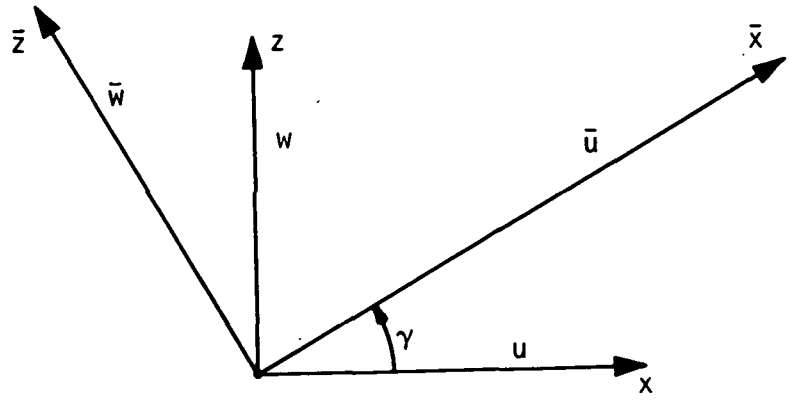

Figure 6. Notation for Streamline (Barred) and Body (Unbarred) Coordinates.

where

$$\gamma = \tan^{-1}\left(\frac{w_e}{u_e}\right) \tag{2.2.6}$$

On the attachment line the coordinate directions coincide, so that

$$u \equiv \bar{u} \qquad \text{and} \qquad w = \bar{w} = 0$$

An expression for w_z can be obtained by making use of the expressions

$$\sin\gamma = \frac{w_e}{u_s}, \qquad \cos\gamma = \frac{u_e}{u_s}$$

and by taking limit of (2.2.5b) as $z \to 0$. The result is

$$w_z \equiv \frac{\partial w}{\partial z} = \frac{\bar{u}}{u_s}\frac{\partial w_e}{\partial z} + \frac{\partial \bar{w}}{\partial \bar{z}}\frac{d\bar{z}}{dz}$$

But, in the limit,

$$\bar{h}_2 d\bar{z} = h_2 dz$$

or

$$w_z = \frac{\bar{u}}{u_s}\frac{\partial w_e}{\partial z} + \frac{\partial \bar{w}}{\partial \bar{z}}\frac{h_2}{\bar{h}_2} \tag{2.2.7}$$

2.3 Transformation of the Governing Equations

In this section we shall consider the transformed form of the governing equations discussed in the previous two sections. Although those equations can be solved in their physical coordinates x, y, z, it is often convenient to solve them after they have been expressed in terms of transformed coordinates. In problems where the computer storage becomes important, the choice of using transformed coordinates becomes necessary, as well as convenient, since the transformed coordinates allow large steps to be taken in the x and z directions. The reason is that the profiles expressed in the transformed coordinates do not change as rapidly as they do when they are expressed in physical coordinates. In addition, the use of transformed coordinates stretches the coordinate normal to the flow and takes out much of the variation in boundary-layer thickness for laminar flows.

2.3.1 Streamline Coordinates

Following Moore (ref. 6), we define a two-component vector potential such that

$$\rho h_2 u = \frac{\partial \psi}{\partial y}, \qquad \rho h_1 w = \frac{\partial \phi}{\partial y} \tag{2.3.1a}$$

$$h_1 h_2 \overline{\rho v} = -\left(\frac{\partial \psi}{\partial x} + \frac{\partial \phi}{\partial z}\right) + h_1 h_2 (\rho v)_w \tag{2.3.1b}$$

We note that equation (2.3.1b) includes the effect of mass transfer and decouples the wall boundary conditions.

We also define the following transformations:

$$x = x, \qquad z = z, \qquad d\eta = \left(\frac{u_s}{\rho_s \mu_s x}\right)^{1/2} \rho dy \tag{2.3.2a}$$

$$\psi = (\rho_s \mu_s u_s x)^{1/2} h_2 f(x, z, \eta) \tag{2.3.2b}$$

$$\phi = (\rho_s \mu_s u_s x)^{1/2} h_1 g(x, z, \eta) \tag{2.3.2c}$$

Introducing the expressions given by (2.3.1) and (2.3.2) into (2.1.2) to (2.1.4) and making use of the relations given by (2.1.6), we get

Streamwise Momentum

$$[C(1 + \varepsilon_x^+)f'']' + \frac{P_1}{h_1}\left[\frac{\rho_s}{\rho} - (f')^2\right] + P_2 f f'' + (R + N + 2M)\frac{f''g}{2h_2} - K_1 x (g')^2 - (M + N)\frac{f'g'}{h_2} - \frac{(\rho v)_w}{\rho_s u_s} R_s^{1/2} f'' = \frac{x}{h_1}\left(f' \frac{\partial f'}{\partial x} - f'' \frac{\partial f}{\partial x}\right) + \frac{x}{h_2}\left(g' \frac{\partial f'}{\partial z} - f'' \frac{\partial g}{\partial z}\right) \tag{2.3.3}$$

Cross-Flow Momentum

$$[C(1 + \varepsilon_z^+)g'']' - \frac{N}{h_2}(g')^2 + (R + N + 2M)\frac{gg''}{2h_2} + P_2 f g'' + \left(K_1 x - \frac{P_1}{h_1}\right) f'g' - \frac{M}{h_2}\left[\frac{\rho_s}{\rho} - (f')^2\right] - \frac{(\rho v)_w}{\rho_s u_s} R_s^{1/2} g'' = \frac{x}{h_1}\left(f' \frac{\partial g'}{\partial x} - g'' \frac{\partial f}{\partial x}\right) + \frac{x}{h_2}\left(g' \frac{\partial g'}{\partial z} - g'' \frac{\partial g}{\partial z}\right) \tag{2.3.4}$$

Energy

$$\left\{C\left[\left(1+\varepsilon^{+}\frac{Pr}{Pr_t}\right)\frac{\theta'}{Pr}+\frac{u_s^2}{H_s}\left(1-\frac{1}{Pr}\right)(f'f''+g'g'')\right]\right\}' + P_2 f\theta' + (R+N+2M)\frac{g\theta'}{2h_2}$$

$$-\frac{(\rho v)_w}{\rho_s u_s} R_s^{1/2}\theta' = \frac{x}{h_1}\left(f'\frac{\partial\theta}{\partial x}-\theta'\frac{\partial f}{\partial x}\right)+\frac{x}{h_2}\left(g'\frac{\partial\theta}{\partial z}-\theta'\frac{\partial g}{\partial z}\right) \qquad (2.3.5)$$

where the primes denote differentiation with respect to η and

$$f' = \frac{u}{u_s}, \qquad g' \equiv \frac{w}{u_s}, \qquad \theta \equiv \frac{H}{H_s}, \qquad R_s = \frac{u_s x}{\nu_s}, \qquad C = \frac{\rho\mu}{\rho_s\mu_s}$$

$$P_1 \equiv \frac{x}{u_s}\frac{\partial u_s}{\partial x}, \quad M \equiv -K_2 h_2 x \quad S = \frac{x}{\rho_s\mu_s}\frac{\partial}{\partial x}(\rho_s\mu_s), \quad R = \frac{x}{\rho_s\mu_s}\frac{\partial}{\partial z}(\rho_s\mu_s)$$

$$N = \frac{x}{u_s}\frac{\partial u_s}{\partial z} \qquad P_2 = (1+P_1+S-2K_1h_1x)\frac{1}{2h_1} \qquad (2.3.6)$$

In the above equations we have used Boussinesq's eddy-viscosity and eddy-conductivity concepts in order to satisfy the closure conditions for the Reynolds stresses. They are defined by

$$-\rho\overline{u'v'} = \rho\varepsilon_x\frac{\partial u}{\partial y}, \quad -\rho\overline{w'v'} = \rho\varepsilon_z\frac{\partial w}{\partial y}, \quad -\rho\overline{H'v'} = \rho\varepsilon_\theta\frac{\partial H}{\partial y} \qquad (2.3.7a)$$

The turbulent Prandtl number and the dimensionless transport coefficients are defined by

$$Pr_t = \frac{\varepsilon^{+}}{\varepsilon_\theta^{+}}, \qquad \varepsilon^{+} = \frac{\varepsilon}{\nu}, \quad \varepsilon = \left(\varepsilon_x^{+2}+\varepsilon_z^{+2}\right)^{1/2} \qquad \varepsilon_\theta^{+} = \frac{\varepsilon_\theta}{\nu} \qquad (2.3.7b)$$

The boundary conditions (2.1.7) become

$$\eta = 0 \qquad f = g = 0, \qquad f' = g' = 0, \qquad \theta = \theta_w \quad \text{or} \quad \theta' = \theta_w'$$

$$\eta \to \eta_\infty \qquad f' \to 1 \qquad g' \to 0 \qquad \theta \to 1 \qquad (2.3.8)$$

The attachment-line equations can also be transformed by a similar procedure. This time,we define the two-component vector potential by

$$\rho h_2 u = \frac{\partial\psi}{\partial y}, \quad \rho h_1 w_z = \frac{\partial\phi}{\partial y}, \quad h_1h_2\overline{\rho v} = -\left(\frac{\partial\psi}{\partial x}+\phi\right)+h_1h_2(\rho v)_w \qquad (2.3.9)$$

and again use the expressions given by (2.3.2). Introducing the expressions (2.3.9) and (2.3.2) into (2.1.9) to (2.1.11), we get

Streamwise Momentum

$$[C(1 + \varepsilon_x^+)f'']' + \frac{P_1}{h_1}\left[\frac{\rho_s}{\rho} - (f')^2\right] + P_2 ff'' + \frac{x}{h_2} gf'' - \frac{(\rho v)_w}{\rho_s u_s} R_s^{1/2} f'' = \frac{x}{h_1}\left(f' \frac{\partial f'}{\partial x} - f'' \frac{\partial f}{\partial x}\right) \tag{2.3.10}$$

Cross-Flow Momentum

$$[C(1 + \varepsilon_z^+)g'']' + \frac{x}{h_2}[gg'' - (g')^2] + P_2 fg'' + \left(K_1 x - \frac{P_1}{h_1}\right) f'g' + x \frac{\partial K_2}{\partial z}\left[\frac{\rho_s}{\rho} - (f')^2\right] - \frac{(\rho v)_w}{\rho_s u_s} R_s^{1/2} g'' = \frac{x}{h_1}\left(f' \frac{\partial g'}{\partial x} - g'' \frac{\partial f}{\partial x}\right) \tag{2.3.11}$$

Energy

$$\left\{C\left[\left(1 + \varepsilon^+ \frac{Pr}{Pr_t}\right)\frac{1}{Pr}\theta' + \frac{u_s^2}{H_s}\left(1 - \frac{1}{Pr}\right) f'f''\right]\right\}' + P_2 f\theta' + \frac{x}{h_2} g\theta' - \frac{(\rho v)_w}{\rho_s u_s} R_s^{1/2}\theta' = \frac{x}{h_1}\left(f' \frac{\partial \theta}{\partial x} - \theta' \frac{\partial f}{\partial x}\right) \tag{2.3.12}$$

where the definitions of the terms are the same as those defined in (2.3.6), except for g', which is equal to w_z/u_s.

The boundary conditions (2.1.12) become

$$\eta = 0, \quad f = g = 0, \quad f' = g' = 0, \quad \theta = \theta_w \quad \text{or} \quad \theta' = \theta'_w \tag{2.3.13a}$$

$$\eta \to \eta_\infty \qquad f' = \theta = 1, \qquad g' = 0 \tag{2.3.13b}$$

2.3.2 Body Coordinates

The relations used to transform the equations in body coordinates are similar to those used in the previous section. For the general case, we again use the two-component vector potential defined by (2.3.1) and the same relations defined by (2.3.2a,b), except that now the subscript s is replaced by e, that is,

$$d\eta = \left(\frac{u_e}{\rho_e \mu_e x}\right)^{1/2} \rho \, dy \tag{2.3.14}$$

$$\psi = (\rho_e \mu_e u_e x)^{1/2} \, h_2 f(x, z, \eta) \tag{2.3.15a}$$

and ϕ is defined by

$$\phi = (\rho_e \mu_e u_e x)^{1/2} \, h_1 \left(\frac{w_e}{u_e}\right) g(x, z, \eta) \tag{2.3.15b}$$

With these relations and with those given by (2.2.1), we can write (2.1.2) to (2.1.4) as

x-Momentum

$$\begin{aligned}[C(1 + \varepsilon_x^+)f'']' + P_2 ff'' + P_3 g f'' + \frac{M}{h_1}\left[\frac{\rho_e}{\rho} - (f')^2\right] + P_4\left[\frac{\rho_e}{\rho} - (g')^2\right] \\ + P_5\left[g'f' - \frac{\rho_e}{\rho}\right] - \frac{(\rho v)_w}{\rho_e u_e} R_x^{1/2} f'' = \frac{x}{h_1}\left(f' \frac{\partial f'}{\partial x} - f'' \frac{\partial f}{\partial x}\right) \\ + \frac{w_e}{u_e}\frac{x}{h_2}\left(g' \frac{\partial f'}{\partial z} - f'' \frac{\partial g}{\partial z}\right)\end{aligned} \tag{2.3.16}$$

z-Momentum

$$\begin{aligned}[C(1 + \varepsilon_z^+)g'']' + P_2 f g'' + P_3 g g'' + P_6\left[\frac{\rho_e}{\rho} - (f')^2\right] + \frac{w_e}{u_e}\frac{P}{h_2}\left[\frac{\rho_e}{\rho} - (g')^2\right] \\ + P_7\left[g'f' - \frac{\rho_e}{\rho}\right] - \frac{(\rho v)_w}{\rho_e u_e} R_x^{1/2} g'' = \frac{x}{h_1}\left(f' \frac{\partial g'}{\partial x} - g'' \frac{\partial f}{\partial x}\right) \\ + \frac{w_e}{u_e}\frac{x}{h_2}\left(g' \frac{\partial g'}{\partial z} - g'' \frac{\partial g}{\partial z}\right)\end{aligned} \tag{2.3.17}$$

Energy

$$\begin{aligned}\left\{C\left[\left(1 + \varepsilon^+ \frac{Pr}{Pr_t}\right)\frac{\theta'}{Pr} + \frac{u_e^2}{H_e}\left(1 - \frac{1}{Pr}\right)\left(f'f'' + \frac{w_e^2}{u_e^2} g'g''\right)\right]\right\}' + P_2 f\theta' + P_3 g\theta' \\ - \frac{(\rho v)_w}{\rho_e u_e} R_x^{1/2}\theta' = \frac{x}{h_1}\left(f' \frac{\partial \theta}{\partial x} - \theta' \frac{\partial f}{\partial x}\right) + \frac{w_e}{u_e}\frac{x}{h_2}\left(g' \frac{\partial \theta}{\partial z} - \theta' \frac{\partial g}{\partial z}\right)\end{aligned} \tag{2.3.18}$$

where

$$f' = u/u_e, \quad g' = w/w_e, \quad \theta = H/H_e, \quad R_x = u_e x/\nu_e$$

$$M = \frac{x}{u_e}\frac{\partial u_e}{\partial x}, \quad N = \frac{x}{u_e}\frac{\partial u_e}{\partial z}, \quad P = \frac{x}{w_e}\frac{\partial w_e}{\partial z}, \quad Q = \frac{x}{w_e}\frac{\partial w_e}{\partial x}$$

$$S = \frac{x}{\rho_e \mu_e}\frac{\partial}{\partial x}(\rho_e \mu_e) \qquad R = \frac{x}{\rho_e \mu_e}\frac{\partial}{\partial z}(\rho_e \mu_e)$$

$$P_2 = (1 + M + S - 2K_1 h_1 x)\frac{1}{2h_1} \tag{2.3.19}$$

$$P_3 = \frac{w_e}{u_e}\frac{1}{2h_2}(2P - N + R - 2K_2 h_2 x)$$

$$P_4 = \left(\frac{w_e}{u_e}\right)^2 K_1 x, \qquad P_5 = -\frac{w_e}{u_e}\frac{1}{h_2}(-K_2 h_2 x + N), \qquad P_6 = \frac{u_e}{w_e} K_2 x$$

$$P_7 = (K_1 h_1 x - Q)\frac{1}{h_1}$$

The boundary conditions (2.2.2) become

$$\eta = 0 \qquad f = g = 0 \qquad f' = g' = 0 \qquad \theta = \theta_w \text{ or } \theta' = \theta'_w \tag{2.3.20a}$$

$$\eta \to \eta_\infty \qquad f' = g' = 1 \qquad \theta = 1 \tag{2.3.20b}$$

The attachment-line equations can also be transformed by a similar procedure. We define the two-component vector by the relations given by (2.3.9) and again use the relations (2.3.14), except that now we define ϕ by

$$\phi = (\rho_e \mu_e u_e x)^{1/2} h_1 \frac{w_{ze}}{u_e} g(x, z, \eta) \tag{2.3.21}$$

Introducing the expressions (2.3.9), (2.3.14a,b), and (2.3.21) into (2.1.26), (2.1.27), and (2.1.11), we get

x-Momentum

$$[C(1 + \varepsilon_x^+)f'']' + P_2 ff'' + \frac{P_1}{h_2} g f'' + \frac{M}{h_1}\left[\frac{\rho_e}{\rho} - (f')^2\right] - \frac{(\rho v)_w}{\rho_e u_e} R_x^{1/2} f''$$

$$= \frac{x}{h_1}\left(f'\frac{\partial f'}{\partial x} - f''\frac{\partial f}{\partial x}\right) \tag{2.3.22}$$

z-Momentum

$$[C(1 + \varepsilon_z^+)g'']' + P_2 f g'' + \frac{P_1}{h_2} g g'' + P_8\left(f'g' - \frac{\rho_e}{\rho}\right) + \frac{P_1}{h_2}\left[\frac{\rho_e}{\rho} - (g')^2\right] + P_9\left[\frac{\rho_e}{\rho} - (f')^2\right] - \frac{(\rho v)_w}{\rho_e u_e} R_x^{1/2} f'' = \frac{x}{h_1}\left(f' \frac{\partial g'}{\partial x} - g'' \frac{\partial f}{\partial x}\right) \tag{2.3.23}$$

Energy

$$\left\{C\left[\left(1 + \varepsilon^+ \frac{Pr}{Pr_t}\right)\frac{\theta'}{Pr} + \frac{u_e^2}{H_e}\left(1 - \frac{1}{Pr}\right) f f''\right]\right\}' + P_2 f\theta' + \frac{P_1}{h_2} g\theta' - \frac{(\rho v)_w}{\rho_e u_e} R_x^{1/2}\theta' = \frac{x}{h_1}\left(f' \frac{\partial \theta}{\partial x} - \theta' \frac{\partial f}{\partial x}\right) \tag{2.3.24}$$

where

$$f' = u/u_e, \qquad g' = w_z/w_{ze}, \qquad \theta = H/H_e$$

$$P_8 = \left(K_1 h_1 x - \frac{x}{w_{ze}} \frac{\partial w_{ze}}{\partial x}\right)\frac{1}{h_1} \qquad P_1 = \frac{x}{u_e}\frac{\partial w_e}{\partial z} \qquad P_9 = \frac{x u_e}{w_{ze}}\frac{\partial K_2}{\partial z} \tag{2.3.25}$$

The boundary conditions are

$$\eta = 0 \qquad f = g = 0 \qquad f' = g' = 0 \qquad \theta = \theta_w \text{ or } \theta' = \theta_w \tag{2.3.26a}$$

$$\eta = \eta_\infty \qquad f' = g' = \theta = 1 \tag{2.3.26b}$$

III. KELLER'S BOX METHOD

The governing boundary-layer equations presented in the previous chapter form a system of coupled nonlinear partial differential equations that are quite difficult to solve. For a multicomponent gas, their solution is even more dif difficult because, in addition to mass-continuity, momentum, and energy equations, we have a number of species-continuity equations to consider. The solution of those equations for general configurations such as those that occur in aircraft and space shuttle design requires a very efficient, fast, and accurate numerical method with suitable models for the Reynolds stresses.

In this chapter we shall discuss the efficiency, speed and accuracy of a two-point finite-difference method developed by H. B.Keller (ref. 1) and applied to the boundary-layer equations by Keller and Cebeci (refs. 2,3). We shall investigate the computation time and accuracy and the stability properties of this method for two-dimensional incompressible laminar and turbulent flows as well as for three-dimensional laminar flows. On the basis of that information, in Chapter V, we shall estimate the computation time for three-dimensional laminar and turbulent boundary layers of a multicomponent gas, and we shall outline an efficient procedure for solving those equations. But, first, we shall present a brief description of the Box Method and point out the several advantages of that method over the numerical methods now being used for boundary-layer calculations. For simplicity, we shall consider the infinite swept-wing equations for an incompressible flow.

3.1 Box Method for Infinite Swept-Wing Equations

The transformed boundary-layer equations for an incompressible flow over an infinite swept wing follow from (2.3.16) and (2.3.17). With $h_1 = h_2 = 1$ and spanwise derivatives of the form $\partial/\partial z$ being zero, they are

Chordwise Momentum

$$(bf'')' + P_2 ff'' + M[1 - (f')^2] = x\left(f' \frac{\partial f'}{\partial x} - f'' \frac{\partial f}{\partial x}\right) \qquad (3.1.1)$$

Spanwise Momentum

$$(cg'')' + \frac{1}{2} fg'' = x\left(f' \frac{\partial g'}{\partial x} - g'' \frac{\partial f}{\partial x}\right) \qquad (3.1.2)$$

where

$$b = 1 + \varepsilon_x^+, \qquad c = 1 + \varepsilon_z^+, \qquad P_2 = \frac{1 + M}{2} \qquad (3.1.3)$$

We first write the two momentum equations in terms of a first-order system of partial differential equations. For that purpose we introduce new independent variables $u(x,\eta)$, $v(x,\eta)$, $w(x,\eta)$, and $t(x,\eta)$ so that we can write (3.1.1) and (3.1.2) as

$$f' = u \tag{3.1.4a}$$

$$u' = v \tag{3.1.4b}$$

$$g' = w \tag{3.1.4c}$$

$$w' = t \tag{3.1.4d}$$

$$(bv)' + P_2 fv + M(1 - u^2) = x\left(u\frac{\partial u}{\partial x} - v\frac{\partial f}{\partial x}\right) \tag{3.1.4e}$$

$$(ct)' + \frac{1}{2} ft = x\left(u\frac{\partial w}{\partial x} - t\frac{\partial f}{\partial x}\right) \tag{3.1.4f}$$

We next consider the net rectangle shown in figure 7. We denote the net points by

$$x_0 = 0, \qquad x_n = x_{n-1} + k_n, \qquad n = 1, 2, \ldots, N \tag{3.1.5}$$

$$\eta_0 = 0 \qquad \eta_j = \eta_{j-1} + h_j, \qquad j = 1, 2, \ldots, J \qquad \eta_J = \eta_\infty$$

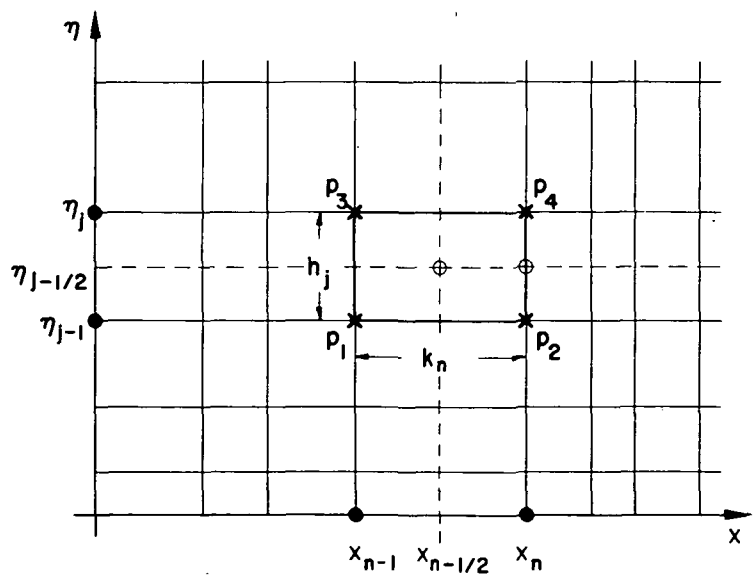

Figure 7. Net Rectangle for the Difference Equations

The net spacings, k_n and h_j, are completely arbitrary and indeed may have large variations in practical calculations. Such flexibility is especially convenient in turbulent boundary-layer calculations, which are characterized by large boundary-layer thicknesses. To get accuracy near the wall, small net spacing is required; large spacing can be used away from the wall.

We approximate the quantities (f, u, v, g, w, t) at points (x_n, η_j) of the net by net functions denoted by $(f_j^n, u_j^n, v_j^n, g_j^n, w_j^n, t_j^n)$. We also employ the notation, for points and quantities midway between net points and for <u>any</u> net function q_j^n:

$$x_{n-1/2} \equiv \frac{1}{2}(s_n + s_{n-1}), \qquad \eta_{j-1/2} \equiv \frac{1}{2}(\eta_j + \eta_{j-1})$$
$$q_j^{n-1/2} \equiv \frac{1}{2}(q_j^n + q_j^{n-1}), \qquad q_{j-1/2}^n \equiv \frac{1}{2}(q_j^n + q_{j-1}^n) \tag{3.1.6}$$

The difference equations that are to approximate (3.1.4) are now easily formulated by considering one mesh rectangle as in figure 7. We approximate (3.1.4a) to (3.1.4d) using centered difference quotients and average about the midpoint $(x_n, \eta_{j-1/2})$ of the segment P_2P_4, with the following results:

$$\frac{f_j^n - f_{j-1}^n}{h_j} = u_{j-1/2}^n \tag{3.1.7a}$$

$$\frac{u_j^n - u_{j-1}^n}{h_j} = v_{j-1/2}^n \tag{3.1.7b}$$

$$\frac{g_j^n - g_{j-1}^n}{h_j} = w_{j-1/2}^n \tag{3.1.7c}$$

$$\frac{w_j^n - w_{j-1}^n}{h_j} = t_{j-1/2}^n \tag{3.1.7d}$$

Similarly (3.1.4e,f) are approximated by centering on the midpoint $x_{n-1/2}, \eta_{j-1/2}$ of the rectangle $P_1P_2P_3P_4$, which gives

$$\frac{(bv)_j^n - (bv)_{j-1}^n}{h_j} - (M^n + \alpha_n)(u^2)_{j-1/2}^n + (P_2^n + \alpha_n)(fv)_{j-1/2}^n$$

$$+ \alpha_n \left(f_{j-1/2}^n v_{j-1/2}^{n-1} - v_{j-1/2}^n f_{j-1/2}^{n-1}\right) = T_{j-1/2}^{n-1} \qquad (3.1.7e)$$

$$\frac{(ct)_j^n - (ct)_{j-1}^n}{h_j} + (\tfrac{1}{2} + \alpha_n)(ft)_{j-1/2}^n - \alpha_n (uw)_{j-1/2}^n$$

$$- \alpha_n \left(u_{j-1/2}^{n-1} w_{j-1/2}^n - w_{j-1/2}^{n-1} u_{j-1/2}^n - t_{j-1/2}^{n-1} f_{j-1/2}^n\right.$$

$$\left. + f_{j-1/2}^{n-1} t_{j-1/2}^n\right) = S_{j-1/2}^{n-1} \qquad (3.1.7f)$$

where

$$T_{j-1/2}^{n-1} = \alpha_n \left[(fv)_{j-1/2}^{n-1} - (u^2)_{j-1/2}^{n-1}\right] - M^n - \left[\frac{(bv)_j^{n-1} - (bv)_{j-1}^{n-1}}{h_j}\right.$$

$$\left. + M^{n-1}\left\{1 - (u^2)_{j-1/2}^{n-1}\right\} + P_2^{n-1} (fv)_{j-1/2}^{n-1}\right] \qquad (3.1.8a)$$

$$S_{j-1/2}^{n-1} = \alpha_n \left[(ft)_{j-1/2}^{n-1} - (uw)_{j-1/2}^{n-1}\right] - \left[\frac{(ct)_j^{n-1} - (ct)_{j-1}^{n-1}}{h_j} + \frac{1}{2}(ft)_{j-1/2}^{n-1}\right] \qquad (3.1.8b)$$

$$\alpha_n \equiv \frac{x_{n-1/2}}{x_n - x_{n-1}} \qquad (3.1.8c)$$

Equations (3.1.7) are imposed for $j = 1, 2, \ldots, J$. For most laminar flows η_J is constant. For turbulent flows, η_J may be increased, with no essential difficulty, as the calculations proceed downstream from the point of transition.

The boundary conditions for (3.1.1) and (3.1.2) are

$$f_0^n = f_w(x), \quad g_0^n = 0, \quad u_0^n = 0, \quad w_0^n = 0, \quad u_J^n = 1, \quad g_J^n = 1 \qquad (3.1.9)$$

If we assume $(f_j^{n-1}, u_j^{n-1}, v_j^{n-1}, g_j^{n-1}, w_j^{n-1}, t_j^{n-1})$ to be known for $0 \leq j \leq J$, then (3.1.7) for $1 \leq j \leq J$, and the boundary conditions (3.1.9) yield an implicit nonlinear algebraic system of $6J + 6$ equations in as many unknowns $(f_j^n, u_j^n, v_j^n, g_j^n, w_j^n, t_j^n)$. The system can be solved very effectively by using Newton's method. The details are presented in reference 3. The important observations are that the linearized equations obtained by applying Newton's method to (3.1.7) and (3.1.9) form a block tridiagonal system (with 6 x 6 blocks) and that system can be solved very efficiently by the procedure discussed in reference 3.

3.2 Computation Time of the Box Method

We have studied the computation time of the Box Method for two-dimensional laminar and turbulent flows as well as for three-dimensional laminar flows. These studies were made on an IBM 370/165.

From a computational aspect, turbulent boundary layers present a much more difficult problem of calculation than laminar boundary layers. Consider, for example, an incompressible turbulent flow. The skin-friction is appreciably greater than it is for a laminar flow yet the boundary-layer is much thicker. This means that the velocity gradient $\partial u/\partial y$ is greater at the wall. To maintain computational accuracy when $\partial u/\partial y$ is large, short steps in y must be taken; when it is small, longer steps can be taken. Therefore, near the wall the steps in a turbulent boundary layer must be shorter than they are in a laminar boundary layer under similar conditions, yet near the outer edge they can be longer.

The numerical method described in Section 3.1 is unique in that various types of spacings in both x- and y-directions can be used with ease. In the calculations we present in this chapter, we have done the calculations for an arbitrary Δx-spacing but for a particular $\Delta\eta$-spacing. The net in the η-direction is a geometric progression having the property that the ratio of lengths of any two adjacent intervals is a constant; that is, $h_j = Kh_{j-1}$. The distance to the j-th η-line is given by the following formula:

$$\eta_j = h_1 \frac{K^j - 1}{K - 1} \qquad j = 1, 2, 3, \ldots J, \qquad K^2 < 1 \qquad (3.2.1)$$

There are two parameters: h_1, the length of the first $\Delta\eta$-step, and K, the ratio of two successive steps. The total number of points J can be calculated by the following formula:

$$J = \frac{\ell n[1 + (K - 1)\ \eta_\infty/h_1]}{\ell n\ K} \tag{3.2.2}$$

In our calculations we select the parameters h_1 and K and calculate the η_∞.

To study the computation time of the Box Method for two-dimensional turbulent boundary layers, we selected a flat-plate flow. In the range of Reynolds number R_x between 1×10^6 to 40×10^6, 21 x-stations and 50 η-points were computed. The total Central-Processing-Unit time (CPU) was 0.048 min. That time corresponds approximately to 0.14 sec/x-station and to 2.75×10^{-3} sec per η-point and per x-station. In the calculations the wall shear parameter, f''_w, was taken as the convergence parameter. The iterations were repeated until

$$\frac{f''_w(\nu+1) - f''_w(\nu)}{1/2[f''_w(\nu+1) + f''_w(\nu)]} < \gamma_1 \tag{3.2.3}$$

where γ_1 is a small error tolerance parameter. On the average, the calculations required two iterations per x-station with $\gamma_1 = 0.01$.

To study the computation time of the box scheme for a semi-three-dimensional flow, we have considered two different test cases. In one test case we have computed the turbulent boundary layers over a yawed flat-plate approximately in the same Reynolds number range as the two-dimensional test case discussed above. Again 21 x-stations and 50 η-points were taken. The CPU time was 0.085 min. That time corresponds approximately to 0.243 sec/x-station and 4.8×10^{-3} sec per η-point and per x-station. Again in each x-station, calculations required two iterations to satisfy (3.2.3).

In the second test case we have considered the Bradshaw-Terrell flow (ref. 7), which is a flow past a 45° "infinite" swept wing. In that flow, measurements were made only at the rear of the wing in a region of nominally zero-pressure gradient and decaying crossflow. The CPU computation time to

calculate the complete flow field with 20 x-stations and 50 η-points was 0.051 min. That time corresponds to approximately 0.14 sec/x-station and 3×10^{-3} sec per η-point and per x-station. At first, the computation time for this flow appears to be approximately the same as the time for the two-dimensional flow which required 0.048 min. However, the Bradshaw-Terrell flow required approximately one iteration per x-station and 22 iterations for the complete flow. Figure 8 shows a comparison of calculated and experimental results.

The computation time of the Box Method was also studied for a full incompressible three-dimensional laminar flow by considering the flow past a flat plate with attached cylinder (see fig. 9). In this case, the iterations were repeated until

$$\left| f_w''^{(\nu+1)} - f_w''^{(\nu)} \right| < 0.0001 \qquad (3.2.4)$$

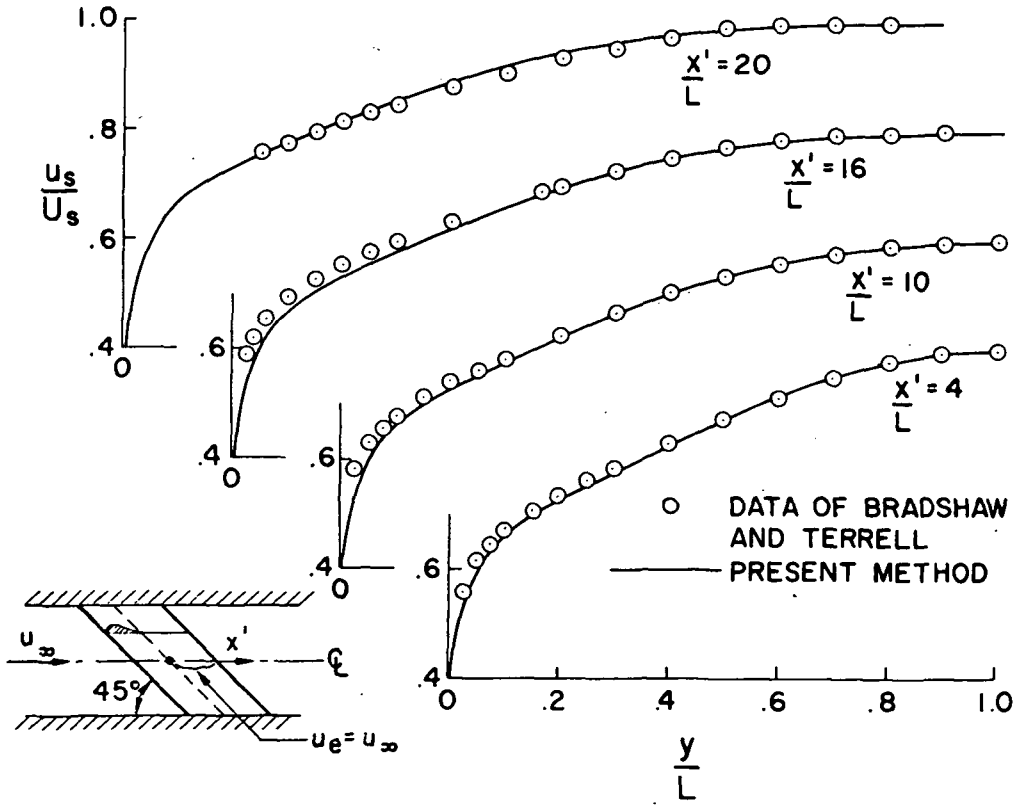

Figure 8. Results for the Relaxing Flow of Bradshaw and Terrell. The Calculations Used the Eddy Viscosity Formulation Described in Chapter IV.

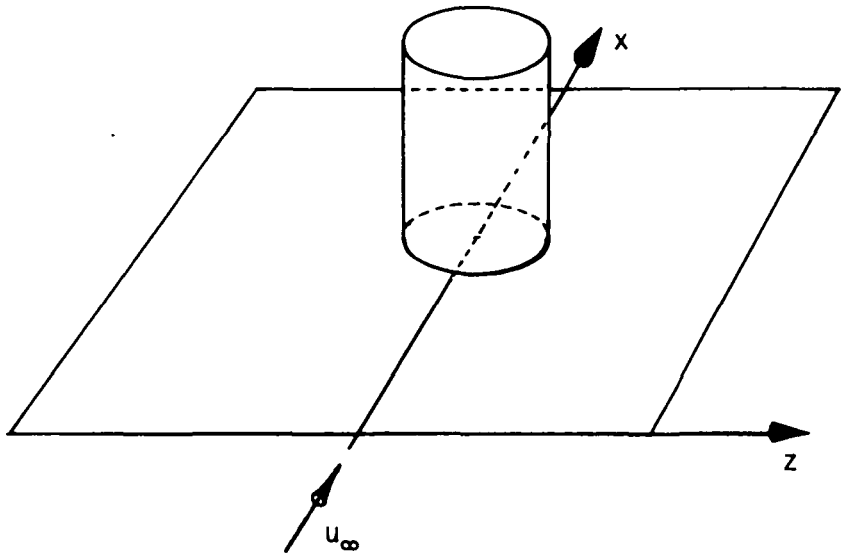

Figure 9. Flow Past a Flat Plate with Attached Cylinder.

The total CPU time for 25 x-stations, 16 z-stations and 21 η-points was 1.285 min. That time corresponds to approximately 3 sec/plane and 9 x 10^{-3} sec per x-station, per z-station, and per η-point. On the average the calculations required 2 to 3 iterations on the attachment line and only 2 iterations away from the attachment line. The results agree quite well with those obtained by Dwyer (ref. 8) and by Fillo and Burbank (ref. 9), who have also studied the same flow using a different finite-difference method.

3.3 Accuracy of the Box Method

The accuracy of the Box Method has been studied for both incompressible and compressible, laminar and turbulent boundary layers past two-dimensional and axisymmetric bodies. Some of the results have been reported in references 2 and 3 and others will be reported in a forthcoming book by Cebeci and Smith. The results indicate that the method is quite accurate and extremely well suited for boundary layers, especially for turbulent flows. Extensive studies with incompressible and compressible turbulent boundary layers show that, in general, 40 to 50 η-points with the Box Method give results which are comparable to the results obtained by the method of reference 11, using 300 to 400 η-points.

The studies in two-dimensional flows also show that one can take relatively large Δx-spacing in the x-direction as long as the equations are solved in terms of the similarity variables similar to the ones discussed in Chapter II. In

general, an airfoil calculation in transformed coordinates requires 20 to 25 x-stations. However, the same calculation in physical coordinates may require 50 to 75 x-stations.

To study the effect of $\Delta\eta$- and Δx-spacings on the results, we have computed the turbulent boundary-layer flow on a flat plate for a Reynolds number range of 10^6 to 10^9. Figure 10 and Table 1 show the skin-friction results with two different $\Delta\eta$- and Δx-spacings. Figure 10 shows the results with fixed $\Delta\eta$-spacing ($h_1 = 0.002$, $K = 1.226$), and with variable Δx-spacing. The latter was chosen such that starting from $R_x = 10^6$, the ΔR_x-spacing of

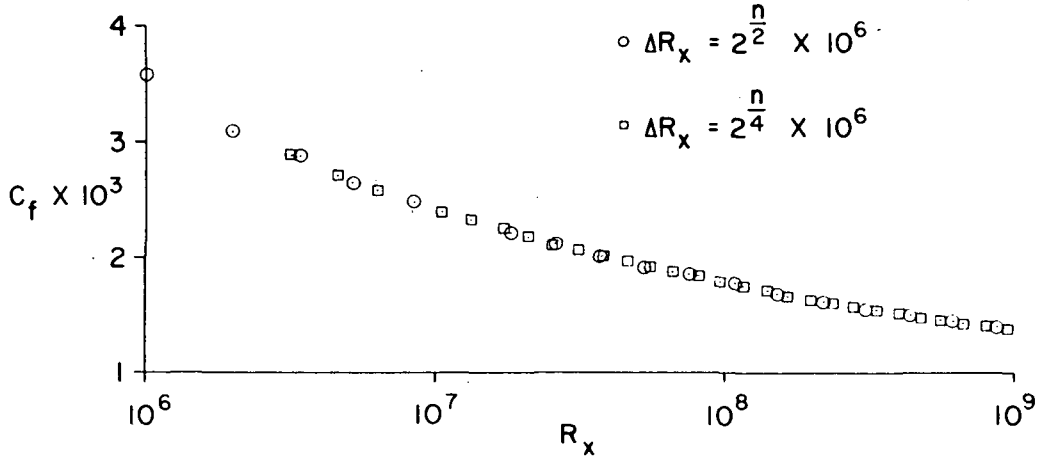

Figure 10. Effect of Δx-Spacing on the Computed c_f-Results. Calculations Were Made for a Fixed $\Delta\eta$-Spacing.

Table 1. Effect of $\Delta\eta$-Spacing on the Computed Results with a Fixed Δx-Spacing. $h_1^{(0)} = 0.002$, $h_2^{(0)} = 0.001$.

$R_x \cdot 10^{-6}$	$c_f(h_1^{(0)})10^3$	$c_f(h_1^{(1)})10^3$	$R_{\theta}(h_1^{(0)})10^3$	$R_{\theta}(h_1^{(1)})10^3$	$c_f(h_1^{(0)},h_1^{(1)})10^3$	$R_{\theta}(h_1^{(0)},h_1^{(1)})10^3$
1.0	3.583	3.570	2.23	2.22	3.566	2.2167
10.7	2.387	2.369	15.2	15.1	2.363	15.0667
115.3	1.745	1.731	115.9	115.1	1.726	114.83
1133.5	1.352	1.329	864.0	850.9	1.321	846.53

$2^{n/2} \times 10^6$ and $2^{n/4} \times 10^6$ gives approximately 20 and 40 x-stations, respectively, in the Reynolds number range under consideration. The results indicate that the c_f-values are not very sensitive to the Δx-spacing.

Table 1 shows the computed c_f and R_θ values for fixed Δx-spacing ($\Delta R_x = 2^{n/4} \times 10^6$) with variable $\Delta\eta$-spacing. The calculations were first made with $h_1 = 0.002$, $K = 1.226$ and then the net points in the η-direction were doubled by halving each $\Delta\eta$-interval.

Table 1 also shows the Richardson-extrapolated values of c_f and R_θ. According to the results, the c_f and R_θ values computed by $h_1^{(0)} = 0.002$ spacing (approximately 50 η-points across the boundary layer) are quite satisfactory.

Figure 11 shows the computed transformed boundary-layer thickness, η_∞, as the calculations proceed downstream (see ref. 10). It is interesting to note that although the η_∞ increases from 20 to 200, the use of the variable grid keeps the number of η-points approximately constant, and the use of the Box Method maintains the computation accuracy in a large range of Reynolds numbers.

3.4 Stability Properties of the Box Method

Currently there are a number of numerical methods used to solve the boundary-layer equations. In reference 11, Blottner gives a general review of these methods. The stability properties of most of these methods, except

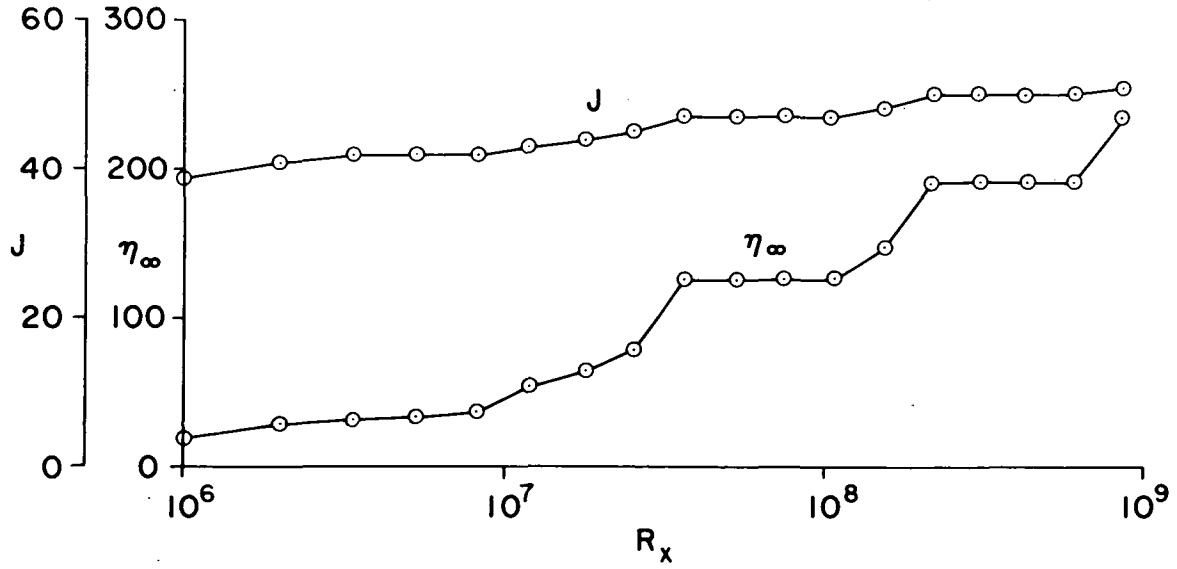

Figure 11. Variation of the Transformed Boundary-Layer Thickness and the Number of η-Points with Reynolds Number.

for the method of Krause, Hirschel and Bothmann (ref. 4), have not been investigated for three-dimensional boundary-layer equations.

It is difficult to compare the stability properties of the schemes of Krause, et al, with those of the box-scheme by the methods used in reference 4. One main reason is that Krause, et al, do not give a complete stability analysis but study only one momentum equation while neglecting some of the convection terms and other coupling terms. The box scheme is based on a different formulation of the boundary-layer equations (requiring them to be replaced by a first-order system and using transformed variables to reduce the variations in the solutions). However, when an analogous linearized stability analysis is made of the box-scheme (ref. 12), dropping terms similar to those neglected in reference 4, the stability properties are found to be at least as good as those of the best scheme of Krause, et al. Indeed even retaining terms that are dropped in reference 4, the analysis shows stability under very general conditions.

Unfortunately, such linearized stability studies cannot be conclusive. The best test would be to solve several difficult problems with each method. We could not make such a comparison in our study because neither the exact difference scheme nor the exact problems treated were specified in reference 4.

However, some important comparisons can be made. Since Krause, et al, always employ three-point differences in the normal (or boundary layer) direction, they must use a uniform net through the boundary layer or else they do not get second-order accuracy. The box-scheme is unrestricted in net spacing, getting not only second-order accuracy but even fourth-order or sixth-order accuracy with only one or two Richardson extrapolations, respectively (ref. 2,3). Also, the Newton iterates used to solve the nonlinear (implicit) equations of the box-scheme converge quadratically and thus are very efficient and do not degrade the accuracy of the solution. It is never clearly spelled out how the nonlinearities are treated in reference 4, so comparisons here are again difficult. Finally, we note that the most stable scheme described by Krause et al does not have second-order accuracy in both tangential directions unless the net spacing is uniform in an appropriate one of these tangential coordinates. Again, there is not such restriction on the box-scheme.

A complete analysis of the three-dimensional boundary-layer equations has never been made. But a preliminary investigation indicates that they are not

stable or well-posed for all tangential flow fields. Indeed something like this must be true since even in two-dimensional flows the boundary-layer equations become unstable when the tangential velocity changes sign (i.e., at separation). For flows in which the boundary-layer equations are not well-posed, it is impossible to devise stable and accurate difference schemes. If the tangential component of the velocity vector turns through a sufficiently large angle, this phenomenon seems to occur. This question should be studied in more detail in order to devise numerical schemes of maximum stability, or indeed to verify if the box-scheme, or any other scheme, possesses maximum stability properties (i.e., is stable whenever the boundary-layer problem is well posed).

IV. TURBULENCE SHEAR MODELS FOR THREE-DIMENSIONAL BOUNDARY LAYERS

The solution of the boundary-layer equations for a turbulent flow requires closure assumptions for the Reynolds stresses. That can be done by a number of approaches*. One approach is to use simple eddy-viscosity and mixing-length formulas for the Reynolds stresses. The methods that use that approach are called mean-flow methods. Typical examples are the methods of Cebeci-Smith (ref. 10), Bushnell-Beckwith (ref. 14), Harris (ref. 15), and Herring and Mellor (ref. 16). Another approach is to use expressions that consider the rate of change of the Reynolds stresses in the governing equations. The methods that use this approach are called transport-equation methods. Typical examples are the methods of Bradshaw (ref. 17) and Donaldson (ref. 18). For low-speed flows, both approaches work equally well. For high-speed flows, however, the mean-flow methods seem to be slightly better than the transport-equation methods, chiefly because of the inadequate closure assumption accounting for the mean compression or dilatation effect. However, a recent report by Bradshaw (Ref. 19) seems to substantially improve the predictions of his method for high-speed flows. In either case, the governing equations for three-dimensional, compressible flows are already quite difficult, and there is no need to increase the complexity of the equations by using higher-order turbulence models. For that reason, we shall restrict our discussion, in this chapter, to the turbulence models that are based on the eddy-viscosity and mixing-length concepts. In particular, we shall describe an eddy-viscosity formulation developed by Cebeci (ref. 20), and compare it with others. We shall also present several results obtained by that formulation. But first, we shall present a brief description of the eddy-viscosity formulation used by Cebeci and Smith for two-dimensional flows.

4.1 Eddy-Viscosity Formulation for Two-Dimensional Compressible Flows

With Boussinesq's eddy-viscosity concept, we can write the Reynolds shear stress, $-\rho\overline{u'v'}$, as

$$-\rho\overline{u'v'} = \rho\varepsilon \frac{\partial u}{\partial y} \tag{4.1.1}$$

---

*For an excellent discussion of various prediction methods, see a recent article by Bradshaw (ref. 13).

According to the eddy-viscosity formulation used by Cebeci and Smith in the so-called inner region of the boundary layer, ε is defined by a modified mixing-length expression. In the outer region ε is defined by an expression based on a velocity defect. For a compressible flow, ε is given by the following formulas:

$$\varepsilon = \begin{cases} L^2 \left|\frac{\partial u}{\partial y}\right| \gamma_{tr} & 0 \leq y \leq y_c \quad (4.1.2a) \\ \alpha \left| \int_0^\infty (u_e - u)dy \right| \gamma_{tr} & y_c \leq y \leq \delta \quad (4.1.2b) \end{cases}$$

where y_c is obtained from the continuity of eddy viscosity. In the above equations, L is a modified mixing-length expression given by

$$L = \kappa y[1 - \exp(-y/A)] \quad (4.1.3)$$

where

$$A = A^+ \frac{\nu}{N} u_\tau^{-1} \left(\frac{\rho}{\rho_w}\right)^{1/2}, \qquad u_\tau = \left(\frac{\tau_w}{\rho_w}\right)^{1/2} \quad (4.1.4a)$$

$$N = \left[\frac{\mu}{\mu_e}\left(\frac{\rho_e}{\rho_w}\right)^2 \frac{P^+}{v_w^+}\left\{1 - \exp\left(11.8 \frac{\mu_w}{\mu} v_w^+\right)\right\} + \exp\left(11.8 \frac{\mu_w}{\mu} v_w^+\right)\right]^{1/2} \quad (4.1.4b)$$

$$v_w^+ = \frac{v_w}{u_\tau}, \qquad P^+ = \frac{\nu_e u_e}{u_\tau^3} \frac{du_e}{dx} \quad (4.1.4c)$$

For flows with no mass transfer N can be written as

$$N = \left[1 - 11.8 \frac{\mu_w}{\mu_e}\left(\frac{\rho_e}{\rho_w}\right)^2 P^+\right]^{1/2} \quad (4.1.4d)$$

According to the study of Cebeci and Mosinskis (ref. 21), the Van Driest damping parameter A^+ and von Karman's parameter κ vary with Reynolds number. Their variation can be approximated by the following empirical formulas:

$$\kappa = 0.40 + \frac{0.19}{1 + 0.49 z_2^2} \quad (4.1.5)$$

$$A^+ = 26 + \frac{14}{1 + z_2^2} \qquad (4.1.6)$$

where $z_2 \equiv R_\theta \times 10^{-3} \geq 0.3$.

The parameter α in the outer eddy-viscosity formula is generally assumed to be a universal constant equal to 0.0168. According to a recent study by Cebeci (ref. 22), however, for values of $R_\theta < 6000$, α is not a universal constant; it varies with R_θ in accordance with the following empirical formula:

$$\alpha = \alpha_o \frac{1 + \Pi_o}{1 + \Pi} \qquad (4.1.7)$$

where $\alpha_o = 0.0168$, $\Pi_o = 0.55$ and Π, which varies from 0 to 1.55 within a R_θ range of 425 to 6000, is approximated by

$$\Pi = 0.55\,[1 - \exp\,(-0.243)\gamma^{1/2} - 0.298\gamma)], \qquad \gamma = \frac{R_\theta}{425} - 1 \qquad (4.1.8)$$

In the definition of γ, the R_θ is defined by

$$R_{\theta_k} = \frac{u_e \theta_k}{\nu_w} \qquad (4.1.9a)$$

where

$$\theta_k = \int_0^\infty \frac{u}{u_e}\left(1 - \frac{u}{u_e}\,dy\right) \qquad (4.1.9b)$$

The low Reynolds number corrections to the eddy-viscosity formulas, given by (4.1.5) to (4.1.9), become quite important at high-speed flows. In a recent study Bushnell and Morris, (ref. 23), analyzed measurements in hypersonic turbulent boundary layers at low Reynolds numbers and observed variations of the parameters κ and α with Reynolds number similar to those given by (4.1.5) and (4.1.7).

The parameter γ_{tr} in the inner and outer eddy-viscosity formulas accounts for the transitional region that exists between a laminar and turbulent boundary layer. It has been used by several authors (refs. 15, 24, 25). According to the expression used by Cebeci (ref. 24), it is given by

$$\gamma_{tr} = 1 - \exp\left[-Gr(x_{tr})\left(\int_{x_{tr}}^{x} \frac{dx}{r}\right)\left(\int_{x_{tr}}^{x} \frac{dx}{u_e}\right)\right] \qquad (4.1.10)$$

where

$$G = \frac{u_e^3}{\nu_e^2} \frac{R_{\theta_{tr}}^{-2.68}}{A^2}, \qquad A = 60 + 4.68M_e^{1.92} \qquad (4.1.11a)$$

Here, x_{tr} and $R_{\theta_{tr}}$ are values taken at the start of transition.

4.2 Extension of the Eddy Viscosity Formulation to Three-Dimensional Compressible Flows

The eddy-viscosity formulation (4.1.2), which is empirical like all models for Reynolds stresses, has worked well for two-dimensional flows. In a recent study by Cebeci, Kaups and Mosinskis (ref. 26), it has also been extended to handle incompressible three-dimensional flows. Here it will be extended to handle compressible flows. In making this extension, we shall rely heavily on our experience with two-dimensional flows and carry over the empirical model used for the viscous layer (ref. 21), to three-dimensional compressible flows. Because of the lack of data on three-dimensional transitional flows, it is difficult to extend the intermittency factor in (4.1.2) to account for the transition region. For that reason, the intermittency factor will not be included in the formulation of eddy viscosity for three-dimensional flows. Furthermore, we shall assume $\varepsilon_x^+ = \varepsilon_z^+$.

For the inner region, we shall assume that the inner-eddy-viscosity formula is given by the following expression:

$$\varepsilon_i = L^2\left[\left(\frac{\partial u}{\partial y}\right)^2 + \left(\frac{\partial w}{\partial y}\right)^2\right]^{1/2} \qquad (4.2.1)$$

Here L is given by (4.1.3) and (4.1.4), except that now the friction velocity u_τ is given by

$$u_\tau = \left(\frac{\tau_{w_s}}{\rho_w}\right)^{1/2}, \qquad \text{where} \quad \frac{\tau_{w_s}}{\rho_w} = \nu_w\left[\left(\frac{\partial u}{\partial y}\right)_w^2 + \left(\frac{\partial w}{\partial y}\right)_w^2\right]^{1/2} \qquad (4.2.2)$$

and the dimensionless pressure-gradient parameter p^+ (uses 2.1.6a) and is given by

$$p^+ = \frac{\nu_s u_s}{u_\tau^3} \frac{\partial u_s}{\partial s} \tag{4.2.3}$$

For the outer region, we shall base the eddy-viscosity expression on a resultant velocity defect defined by

$$u_s - (u^2 + w^2)^{1/2}$$

and we shall write the outer eddy-viscosity expression as

$$\varepsilon_o = \alpha \left| \int_0^\infty [u_s - (u^2 + w^2)^{1/2}] \, dy \right| \tag{4.2.4}$$

Although those inner and outer eddy-viscosity formulas are somewhat speculative, they worked quite well for incompressible flow, (ref. 26), and are recommended for compressible flows until "better" formulas become available.

It should be noted that the proposed expressions for the inner and outer eddy-viscosity formulas do not, in principle, differ from those suggested by Hunt, Bushnell and Beckwith (ref. 27). In a recent study Adams (ref. 28) used those transport coefficients in calculating compressible turbulent boundary layers on sharp cones at incidence and obtained good agreement with experiment.

4.3 Attachment-Line Turbulent Flow on an Infinite Swept Wing

The accuracy of the eddy viscosity presented in Section 4.2 has been thoroughly investigated for incompressible infinite swept wings. The calculated results agreed well with experiment and with those computed by Bradshaw's method (ref. 17). Here, we shall investigate the accuracy of our eddy-viscosity formulation for an incompressible attachment-line turbulent flow on an infinite swept wing.

Figure 12 shows a sketch of potential flow streamlines in attachment-line region of an infinite swept wing, together with the rectangular coordinate system that will be used in this paper. The parameter that determines whether the flow will be laminar or turbulent is a dimensionless parameter defined by

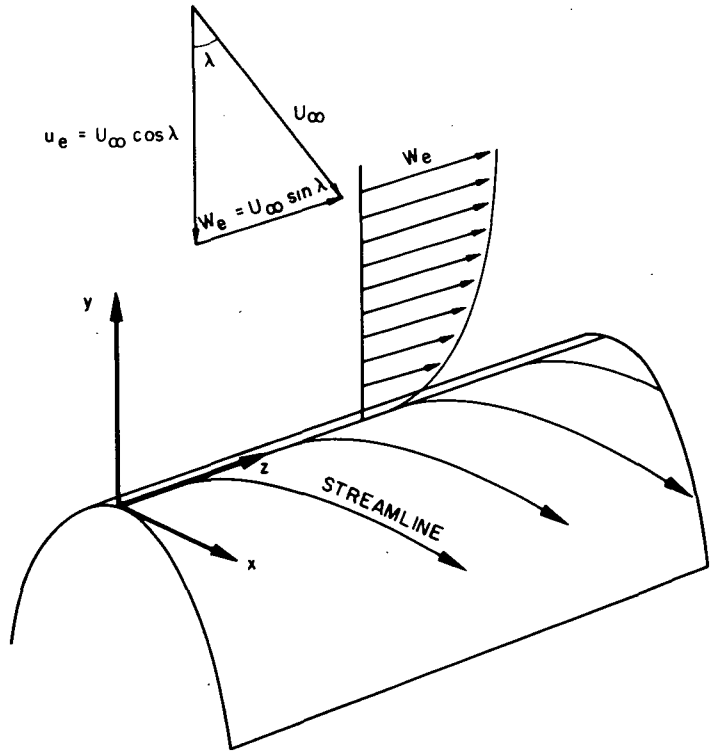

Figure 12. Sketch of Potential-Flow Streamline in Attachment-Line Region of an Infinite Swept Wing and the Coordinate System.

$$C^* = w_e^2 \left(\frac{du_e}{dx} \right)^{-1} \tag{4.3.1}$$

It may be regarded as a Reynolds number with the length scale represented by the ratio of spanwise velocity, w_e, to chordwise velocity gradient, du_e/dx. According to the experiments of Cumpsty and Head (ref. 29), flow along the leading edge is fully turbulent for $C^* > 1.4 \times 10^5$. For $C^* < 0.8 \times 10^5$, the flow is laminar. In the range $0.8 \times 10^5 < C^* < 1.4 \times 10^5$, the flow is transitional.

4.3.1 Governing Boundary-Layer Equations

The governing boundary-layer equations for an incompressible turbulent flow past a yawed infinite wing, with the use of eddy-viscosity concepts can be written as

Continuity

$$\frac{\partial u}{\partial x} + \frac{\partial v}{\partial y} = 0 \tag{4.3.2}$$

Chordwise Momentum

$$u \frac{\partial u}{\partial x} + v \frac{\partial u}{\partial y} = - \frac{1}{\rho} \frac{dp}{dx} + \nu \frac{\partial}{\partial y} \left[(1 + \varepsilon^+) \frac{\partial u}{\partial y} \right] \tag{4.3.3}$$

Spanwise Momentum

$$u \frac{\partial w}{\partial x} + v \frac{\partial w}{\partial y} = \nu \frac{\partial}{\partial y} \left[(1 + \varepsilon^+) \frac{\partial w}{\partial y} \right] \tag{4.3.4}$$

On the attachment line, $u \equiv 0$. Therefore, (4.3.3) is singular along the line (leading edge) $x = 0$. To remove the singularity, we differentiate (4.3.3) with respect to x and set u and $\partial v/\partial x$ equal to zero. That procedure enables (4.3.3) to be written as

$$u_x^2 + v \frac{\partial u_x}{\partial y} = - \frac{1}{\rho} \frac{d^2 p}{dx^2} + \nu \frac{\partial}{\partial y} \left[(1 + \varepsilon^+) \frac{\partial u_x}{\partial y} \right] \tag{4.3.5}$$

where $u_x = \partial u/\partial x$. From Bernoulli's equation it follows that at $x = 0$,

$$- \frac{1}{\rho} \frac{d^2 p}{dx^2} = \left(\frac{du_e}{dx} \right)^2 \tag{4.3.6}$$

Next we introduce a new dependent variable f' defined by

$$f'(\eta) = \lim_{x \to 0} \frac{u}{u_e} = \frac{du}{dx} \left(\frac{du_e}{dx} \right)^{-1} \tag{4.3.7}$$

where the prime on f denotes differentiation with respect to the similarity parameter η defined by

$$\eta = \left(\frac{B}{\nu} \right)^{1/2} y \tag{4.3.8}$$

with $B \equiv (du_e/dx)_{x=0}$.

With (4.3.7) and (4.3.8) we can integrate the continuity equation (4.3.2) and can write it as

$$v = -\sqrt{B\nu}\, f \tag{4.3.9}$$

Substituting the expression for v given by (4.3.9) into (4.3.4) and (4.3.5), and after performing the necessary transformations, we can write the two momentum equations as

Chordwise Momentum

$$(bf'')' + ff'' + 1 - (f')^2 = 0 \tag{4.3.10}$$

Spanwise Momentum

$$(bg'')' + fg'' = 0 \tag{4.3.11}$$

In those equations $b = 1 + \varepsilon^+$ and g' denotes the ratio of w/w_e.

Equations (4.3.10) and (4.3.11) are subject to the following boundary conditions:

at $\eta = 0$

$$f = 0 \qquad \text{or} \qquad -\frac{v_w}{w_e}\sqrt{C^*} \quad \text{(mass transfer)} \tag{4.3.12a}$$

$$f' = g = g' = 0$$

at $\eta = \eta_\infty$

$$f' = g' = 1 \tag{4.3.12b}$$

4.3.2 Eddy-Viscosity Formulation

The eddy-viscosity formulas (4.2.1) and (4.2.4) become

$$\varepsilon_i = (\kappa y)^2 \left[1 - \exp(-y/A)\right]^2 \left|\frac{\partial w}{\partial y}\right| \tag{4.3.13a}$$

$$\varepsilon_o = \alpha \left| \int_0^\infty (w_e - w)dy \right| \tag{4.3.13b}$$

For zero-pressure gradient flow with no mass transfer, the damping length A is

$$A = A^+ \nu \, (\tau_w/\rho)^{-1/2}$$

In terms of transformed variables (4.3.13) can be written as

$$\varepsilon_i^+ = \kappa^2 (C^*)^{1/2} \eta^2 \, |g''| \left[1 - \exp\left(-\frac{\eta |g_w''|^{1/2} (C^*)^{1/4}}{A^+}\right)\right]^2 \tag{4.3.14a}$$

$$\varepsilon_o^+ = \alpha (C^*)^{1/2} \left[\eta_\infty - g_\infty\right] \tag{4.3.14b}$$

In the study reported here, we have used the above eddy-viscosity formulation to compute the fully turbulent boundary layers ($C^* > 1.4 \times 10^5$) on the leading edge of an infinite swept wing. The governing equations, namely, (4.3.10) and (4.3.11), were solved by Keller's Box Method.

When several runs were made for different values of C^*, the solutions indicated very strong oscillations. The oscillations were small at small values of C^*, but they became quite strong at high values of C^*. It should be pointed out that such oscillations are not unusual in turbulent boundary-layer calculations. The appearance of such oscillations arise as a result of the eddy-viscosity formula given by (4.3.13a); they are observed in all numerical methods that use (4.3.13a). However, the oscillations in nonsimilar turbulent flows are quite small and have no bearing on the accuracy of the solutions.

In order to eliminate the oscillations and provide convergence, we have replaced the inner-eddy-viscosity formula (4.3.13a) by another expression,

$$\varepsilon_i = \kappa y^+ [1 - \exp(-y/A)]\nu \tag{4.3.15}$$

which, in terms of transformed variables, can be written as

$$\varepsilon_i^+ = \kappa\eta(g_w''C^*)^{1/2}\left[1 - \exp\left(-\frac{\eta|g_w''^{1/2}|(C^*)^{1/4}}{A^+}\right)\right] \tag{4.3.16}$$

With that change, no oscillations were observed, and the solutions converged quadratically for all values of C^* considered.

4.3.3 Comparison with Experiment

Detailed measurements of attachment-line flows in turbulent boundary layers in incompressible flows are lacking in the literature. The only detailed data known to the authors are the data of Cumpsty and Head (ref. 29). For this reason, our comparison calculations are limited to that data. Figure 13 shows computed and experimental velocity profiles for four values of C^*. The agreement with experiment is quite satisfactory.

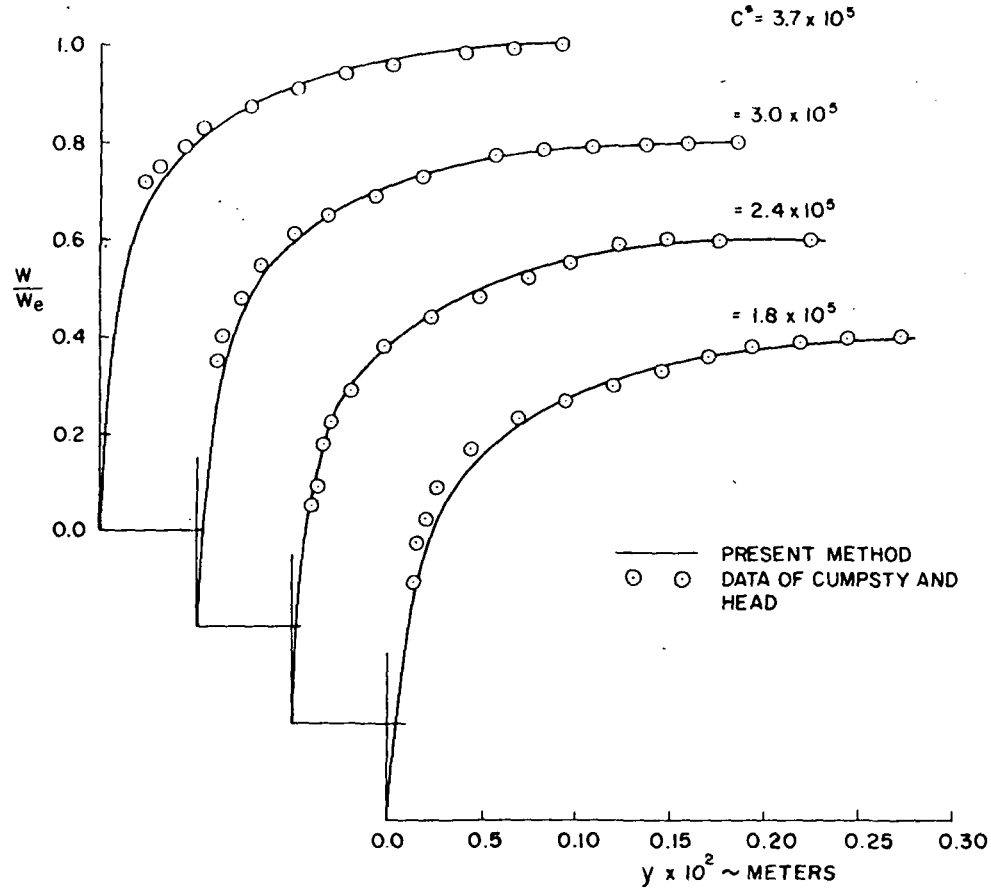

Figure 13. Comparison of Computed and Experimental Velocity Profiles for the Fully Turbulent, Attachment-Line Flow.

As was mentioned before, the flow is fully turbulent only when $C^* > 1.4 \times 10^5$. For the range of $0.8 \times 10^5 < C^* < 1.4 \times 10^5$, the flow is transitional. The calculation for that region was extended by using the intermittency factor γ_{tr} used by Cebeci (ref. 24). For an incompressible flow with zero pressure gradient, it is given by

$$\gamma_{tr} = 1 - \exp\left[-G\left(\frac{x - x_{tr}}{w_e}\right)^2\right] \tag{4.3.17}$$

where G is

$$G = 0.835 \times 10^{-3}\left(\frac{w_e^3}{\nu^2}\right) R_{x_{tr}}^{-1.34} \tag{4.3.18}$$

To have similarity we have written (4.3.17) as

$$\gamma_{tr} = 1 - \exp\left(-Gx_{tr}^2/w_e\right)$$

which, with the use of (4.3.18), can also be written as

$$\gamma_{tr} = 1 - \exp\left[-0.835 \times 10^{-3}(R_x)^{0.66}\right] \qquad (4.3.19)$$

According to a recent study by Bushnell and Alston (ref. 30), in calculating transitional boundary layers it is also necessary to account for the low Reynolds number effect (if there is one) in addition to the intermittent behavior of the flow. An examination of the experimental data of Cumpsty and Head shows that for the range of $0.8 \times 10^5 < C^* < 1.4 \times 10^5$, The Reynolds number based on θ varies between 200 and 400. Now the correction to α in (4.1.7), which is for a low Reynolds number, applies for R_θ greater than 425. For lower R_θ values, we simply extrapolate that curve as shown in figure 14 with a dashed line. The resulting $(\alpha - R)$-curve can be approximated by the following formula:

$$\alpha \times 10^3 = 194.8 - 128.6\,(\log_{10}R_\theta) + 30.925\,(\log_{10}R_\theta)^2 - 2.475\,(\log_{10}R_\theta)^3 \qquad (4.3.20)$$

for $10^2 < R_\theta < 10^4$.

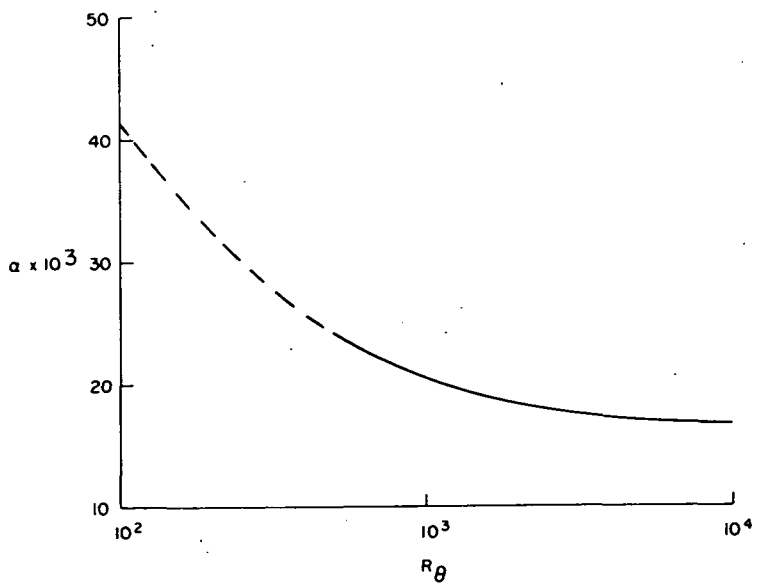

Figure 14. Variation of α with Reynolds Number.

Figure 15 shows the transitional boundary layer profiles, together with the experimental data of Cumpsty and Head (ref. 29). Those calculations were made by multiplying the right-hand side of (4.3.14b) and (4.3.16) by (4.3.19) and by varying α in (4.3.14b) as described by (4.3.20). The agreement with experiment is satisfactory.

Figure 16 shows a comparison between calculated and measured local skin-friction values. Again the agreement with experiment is satisfactory.

Finally, we present the computed R_0 and H-values in Table 2 at different C*-values. We also present the experimental R_θ-values given by Cumpsty and Head. The agreement between predicted and measured values is quite good.

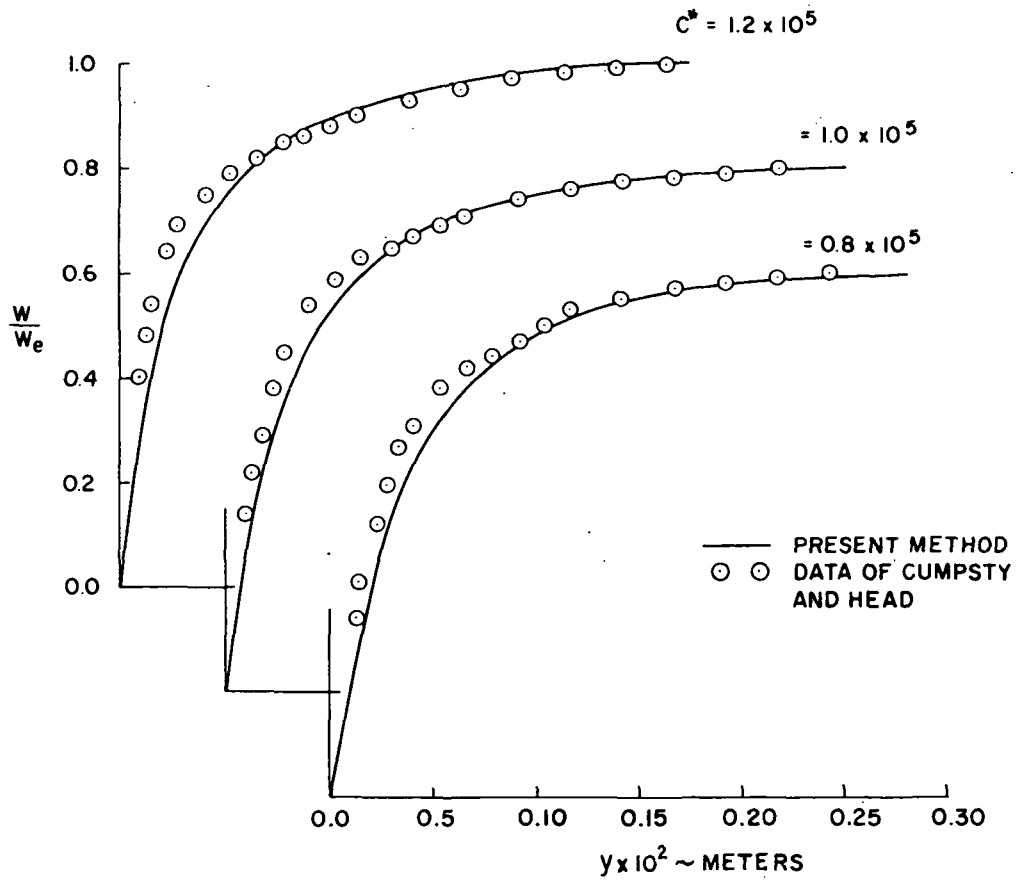

Figure 15. Comparison of Computed and Experimental Velocity Profiles for the Transitional Attachment-Line Flow.

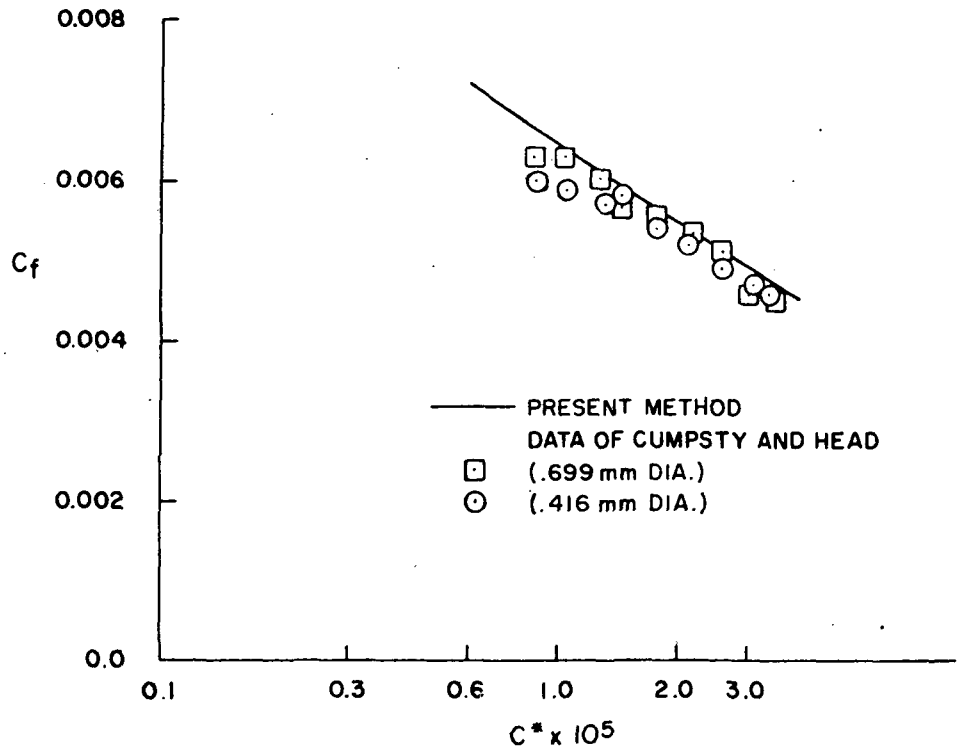

Figure 16. Comparison of Computed and Experimental Skin-Friction Values for the Attachment-Line Flow.

Table 2. R_θ and H-Values for Various C*-Values

	Exp.	Computed	
$C^* \times 10^{-5}$	R_θ	R_θ	H
0.8	200	225	1.76
1.0	250	270	1.71
1.2	295	313	1.68
1.8	430	434	1.60
2.4	540	538	1.57
3.0	640	634	1.55
3.7	760	735	1.53

V. OUTLINE OF A GENERAL METHOD FOR COMPUTING COMPRESSIBLE THREE-DIMENSIONAL MULTICOMPONENT GAS BOUNDARY LAYERS

In this chapter, we shall outline a general method for computing compressible three-dimensional multicomponent gas boundary layers on general configurations. On the basis of the studies conducted in the earlier chapters, we shall give estimates of computation time and computer-storage requirements for a typical space-shuttle configuration. Our estimates are given for an equilibrium or frozen flow consisting of seven-species equations, two momentum equations, one energy, and one continuity equation.

Needless to say, the system of equations under consideration consists of highly coupled nonlinear partial-differential equations. They can be solved efficiently using the Box Method by following the procedure discussed below. In the discussion, we shall assume that the governing equations are expressed in transformed coordinates.

1. Express the system in terms of first-order equations. In our case this procedure yields 22 first-order equations.
2. Approximate the system of 22 first-order equations by the difference equations for the net in figure 7.
3. Linearize the resulting nonlinear algebraic equations by Newton's method and write them in compound-block-matrix-vector notation as

$$\mathbf{A}\,\underset{\sim}{\delta}_j = \underset{\sim}{r}_j \tag{5.1}$$

where

$$\mathbf{A} = \begin{bmatrix} A_0 & C_0 & & & & & \\ B_1 & A_1 & C_1 & & & & \\ & B_2 & A_2 & C_2 & & & \\ & & \cdot & \cdot & \cdot & & \\ & & B_j & A_j & C_j & & \\ & & & \cdot & \cdot & \cdot & \\ & & & B_{J-1} & A_{J-1} & C_{J-1} & \\ & & & & B_J & A_J & \end{bmatrix}, \quad \underset{\sim}{\delta}_j = \begin{bmatrix} \underset{\sim}{\delta}_0 \\ \underset{\sim}{\delta}_1 \\ \cdot \\ \cdot \\ \underset{\sim}{\delta}_j \\ \cdot \\ \cdot \\ \underset{\sim}{\delta}_J \end{bmatrix}, \quad \underset{\sim}{r}_j = \begin{bmatrix} \underset{\sim}{r}_1 \\ \underset{\sim}{r}_2 \\ \cdot \\ \cdot \\ \underset{\sim}{r}_j \\ \cdot \\ \cdot \\ \underset{\sim}{r}_J \end{bmatrix} \tag{5.2}$$

The coefficient matrix A is of order $22J + 22$ and the vectors $\underset{\sim}{\delta}_j$ and $\underset{\sim}{r}_j$ have this dimension. The blocks A_j, B_j, and C_j in the coefficient matrix are of order 22.

4. Solve the system (5.1) by using the block tridiagonal factorization procedure discussed in reference 31.

To estimate the computer storage and computation time for the Box-scheme applied to three-dimensional boundary-layer problems, we suppose there are J intervals in the η-direction, N intervals in the x-direction and K intervals in the z-direction. For example, we feel that $N = 100$, $K = 50$ and $J = 50$ would more than suffice to compute a complete flow field using transformed coordinates. The number of basic variables that enter at each net point, (x_n, z_k, η_j) is $M \equiv (8 + 2S)$ where S is the number of species to be included. Specifically, we introduce three variables for each of the x- and z-momentum equations, two variables for the energy equation and two variables for each species conservation equation (so that each of the equations can be reduced to a first-order system). Using $S = 7$ species yields the $M = 22$ basic variable alluded to in steps 1 - 4 above.

Since each basic variable requires 4 bytes, it is clear that all of the basic variables cannot be stored in the high-speed memory at the same time. This would require for the maximum net cited above, $N \times K \times J \times 4 \times M = 22 \times 10^6$ bytes or 22×10^3 K-bytes of memory. However, by efficient organization of the computer program we need only retain at one time all those basic variables on at most 5 "η-columns" [i.e., all points (x_n, z_k, η_j) with fixed (x_n, z_k) and all j in $0 \leq j \leq J$]. This requires at most $5 \times J \times 4 \times M = 22 \times 10^3$ bytes = 22 K-bytes of high-speed memory. While the solution on one η-column is being computed, the data on the next required η-column is being read in from auxiliary storage (i.e., disks) and the last computed column is being stored. This overlay technique may substantially reduce the delay time in data transfer. There is no difficulty in allowing as many as 50 K-bytes for the five columns to include fluid properties and other parameters.

To estimate computation time, we recall that one η-column is obtained by solving the linear system (5.1) once for each Newton iteration. The matrix elements of A and the inhomogeneous term $\underset{\sim}{r}_j$ must also be recomputed for each iterate. The number of operations to compute these quantities is proportional to M^2J while the number of operations to solve (5.1) is proportional

to M^3J. Thus, we note a very strong dependence on M, the number of basic variables to each net point, and only linear dependence on J, the number of intervals across the boundary layer. We recall that the number of η-columns is $N \times K$ so that the total computation time will also be linear in these quantities. Finally, we point out that the computation time is also proportional to the average number of Newton iterates employed for each "column."

For the computations reported in Section 3.2, where $M = 6$, $N = 25$, $K = 16$ and $J = 21$, the total CPU time on an IBM 370/165 was 1.285 minutes. Using the above observed linearity with number of η-intervals if we take $J = 50$ rather than $J = 21$, the time would be $1.285 \times 50/21 = 3$ minutes, approximately. This is probably an overestimate since a refinement in the η-spacing would most likely reduce the required number of iterations. However, this estimate corresponds to about 7.2 sec/(η,z)-plane (or 0.9×10^{-2} sec/net point). Thus, for the case of $M = 22$ (with $S = 7$ species), $N = 25$, and $K = 16$, we estimate:

$$7.2 \times \left(\frac{22}{6}\right)^3 = 6 \text{ minutes/}(\eta,z)\text{-plane}$$

For as many as $J = 50$ η-points through the boundary layer, this yields five hours for the total computation. If we wish to use $N = 100$ and $K = 50$ we get the tremendous estimate of 125 hours of CPU time.

This is unrealistic for practical computations. Fortunately, there are several ways in which we can significantly reduce the required computation time. First and most basic for Keller's Box-method, is the fact that Richardson's extrapolation can be employed and yields two orders of accuracy improvement per applications. Thus, with at most $N = 50$, $K = 25$ and $J = 25$ points, we can obtain the same accuracy and reduce the computation time by slightly less than a factor of 8. So we consider now that 16 hours of CPU time are required (with $M = 22$).

Another powerful reduction in computation time is obtained by effectively reducing the number of basic variables M that are simultaneously coupled in solving the Box-difference equations. If only the two momentum and energy equations are simultaneously solved, our computing estimate with $M = 8$ applies. Using $N = 100$, $K = 50$, $J = 50$ (i.e., without Richardson's extrapolation), the 125-hour estimate is now reduced to $125 \times (8/22)^3 = 6$ hours. However, the $S = 7$ species equations must each be solved and then their updated values

employed to recompute the momentum and energy quantities. This "inner-outer" iteration procedure should be required at most three times and probably no more than twice. Thus, at most 18 hours should be required by this technique.

If we use the inner-outer iterations only to solve the two momentum equations, i.e., $M = 6$, and then solve separately the energy and species equations, the above estimate reduces to about 7.5 hours. This seems to be the most promising resolution of the difficulty as now the application of Richardson's extrapolation brings us to about one hour of CPU time for an accurate solution.

We cannot tell at the present stage of development how optimistic or pessimistic the above estimates may be. We do feel that they are in the right ball park. It clearly should be one of the major objectives of future work in this area to test alternatives and to devise the most efficient set of procedures.

REFERENCES

1. Keller, H.B.: A New Difference Scheme for Parabolic Problems in "Numerical Solution of Partial Differential Equations." (J. Bramble, Ed.), Vol. II, Academic Press, New York, 1970.
2. Keller, H.B., and Cebeci, T.: Simple Accurate Numerical Methods for Boundary Layers. I. Two-Dimensional Laminar Flows. Proceedings of the Second International Conference on Numerical Methods in Fluid Dynamics. Lecture Notes in Physics, Vol. 8, Springer-Verlag, New York, 1971.
3. Keller, H.B., and Cebeci, T.: Simple Accurate Numerical Methods for Boundary Layers. II. Two-Dimensional Turbulent Flows. AIAA Journal, Vol. 10, No. 9, pp. 1197-1200, September 1972.
4. Krause, E., Hirschel, E.H., and Bothmann, Th.: Die Numerische Integration der Bewegungsgleichungen Dreidimensionaler Laminarer Kompressibler Grenzschichten. Fachtagung Aerodynamik, Berlin, 1968, D6LR-Fachlinchreike, Bond 3, 1969.
5. Squire, L.C.: The Three-Dimensional Boundary-Layer Equations and Some Power Series Solutions. A.R.C. Tech. Rept., R&M No. 3006, 1957.
6. Moore, F.K.: Theory of Laminar Flows. Vol. IV, Princeton University Press, Princeton, New Jersey, 1964.
7. Bradshaw, P., and Terrell, M.G.: The Response of a Turbulent Boundary Layer on an Infinite Swept Wing to the Sudden Removal of Pressure Gradient. Nat. Phys. Lab. Aero Rept. No. 1305, 1969.
8. Dwyer, H.A.: Solution of a Three-Dimensional Boundary-Layer Flow with Separation. AIAA Journal, Vol. 6, No. 7, pp. 1336-1342, July 1968.
9. Fillo, J.A., and Burbank, R.: Calculation of Three-Dimensional Laminar Boundary-Layer Flows. AIAA Journal, Vol. 10, No. 3, pp. 353-355, March 1972.
10. Cebeci, T., and Smith, A.M.O.: A Finite-Difference Method for Calculating Compressible Laminar and Turbulent Boundary Layers. Journal of Basic Engineering, Vol. 92, No. 3, pp. 523-535, August 1970.
11. Blottner, F.G.: Finite-Difference Methods of Solution of the Boundary-Layer Equations. AIAA Journal, Vol. 8, pp. 193-205, February 1970.

12. Keller, H.B.: Unpublished Notes.
13. Bradshaw, P.: The Understanding and Prediction of Turbulent Flow. Aeronautical Journal, pp. 403-416, July 1972.
14. Bushnell, D.M. and Beckwith, I.E.: Calculation of Nonequilibrium Hypersonic Turbulent Boundary Layers and Comparisons with Experimental Data. AIAA Journal, Vol. 8, pp. 1462-1469, August 1970.
15. Harris, J.E.: Numerical Solution of the Equations for Compressible Laminar, Transitional, and Turbulent Boundary Layers and Comparisons with Experimental Data. NASA TR R-368, August 1971.
16. Herring, H.J., and Mellor, G.L.: A Method of Calculating Compressible Turbulent Boundary Layers. NASA CR-1144, 1968.
17. Bradshaw, P.: Calculation of Three-Dimensional Turbulent Boundary Layers. Journal of Fluid Mechanics, Vol. 46, Pt. 3, pp. 417-445, April 1971.
18. Donaldson, C.DuP., and Sullivan, R.D.: An Invariant Second-Order Closure Model of the Compressible Turbulent Boundary Layers on a Flat Plate. A.R.A.P. Rept. No. 178, June 1972.
19. Bradshaw, P.: Anomalous Effects of Pressure Gradient on Supersonic Turbulent Boundary Layers. Imperial College, Aero Rept. 72-21, 1972.
20. Cebeci, T.: Calculation of Compressible Turbulent Boundary Layers with Heat and Mass Transfer. AIAA Journal, Vol. 9, No. 6, pp. 1091-1098, June 1971.
21. Cebeci, T., and Mosinskis, G.J.: Calculation of Incompressible Turbulent Boundary Layers at Low Reynolds Numbers. AIAA Journal, Vol. 9, No. 8, pp. 1632-1634, August 1971.
22. Cebeci, T.: Kinematic Eddy Viscosity at Low Reynolds Numbers. AIAA Journal, Vol. 11, No. 1, pp. 102-104, January 1973.
23. Bushnell, D.M., and Morris, D.J.: Shear Stress, Eddy-Viscosity and Mixing-Length Distributions in Hypersonic Turbulent Boundary Layers. NASA TM X-2310, 1971.
24. Cebeci, T.: Curvature and Transition Effects in Turbulent Boundary Layers. AIAA Journal, Vol. 9, No. 9, September 1971.
25. Adams, J.C., Jr.: Numerical Calculation of Sharp Flat Plate Transitional and Turbulent Skin Friction. AIAA Journal, Vol. 10, No. 6, pp. 841-842, June 1972.

26. Cebeci, T., Mosinskis, G.J., and Kaups, K.: A General Method for Calculating Three-Dimensional Incompressible Laminar and Turbulent Boundary Layers. I. Swept Infinite Cylinders and Small Cross Flow. Douglas Aircraft Co. Rept. MDC J5694, November 1972.

27. Hunt, J.L., Bushnell, D.M., and Beckwith, I.E.: The Compressible Turbulent Boundary Layer on a Blunt Swept Slab with and without Leading-Edge Blowing. NASA TN D-6203, March 1971.

28. Adams, J.C.: Analysis of the Three-Dimensional Compressible Turbulent Boundary Layer on a Sharp Cone at Incidence in Supersonic and Hypersonic Flow. AEDC-TR-72-66, June 1972.

29. Cumpsty, N.A., and Head, M.R.: The Calculation of the Three-Dimensional Turbulent Boundary Layer. Part 3. Comparison of Attachment-Line Calculations with Experiment. The Aeronautical Quarterly, Vol. 20, pp. 99-113, May 1969.

30. Bushnell, D.M., and Alston, D. W.: On the Calculation of Transitional Boundary Layers. AIAA J., vol. 11, no. 4, Apr. 1973, pp. 554-556.

31. Isaacson, E., and Keller, H.B.: Analysis of Numerical Methods. John Wiley & Sons, New York, 1966.

NATIONAL AERONAUTICS AND SPACE ADMINISTRATION
WASHINGTON, D.C. 20546

OFFICIAL BUSINESS
PENALTY FOR PRIVATE USE $300

SPECIAL FOURTH-CLASS RATE
BOOK

POSTAGE AND FEES PAID
NATIONAL AERONAUTICS AND
SPACE ADMINISTRATION
451

U.S.MAIL

POSTMASTER : If Undeliverable (Section 158 Postal Manual) Do Not Return

"The aeronautical and space activities of the United States shall be conducted so as to contribute . . . to the expansion of human knowledge of phenomena in the atmosphere and space. The Administration shall provide for the widest practicable and appropriate dissemination of information concerning its activities and the results thereof."

—NATIONAL AERONAUTICS AND SPACE ACT OF 1958

NASA SCIENTIFIC AND TECHNICAL PUBLICATIONS

TECHNICAL REPORTS: Scientific and technical information considered important, complete, and a lasting contribution to existing knowledge.

TECHNICAL NOTES: Information less broad in scope but nevertheless of importance as a contribution to existing knowledge.

TECHNICAL MEMORANDUMS: Information receiving limited distribution because of preliminary data, security classification, or other reasons. Also includes conference proceedings with either limited or unlimited distribution.

CONTRACTOR REPORTS: Scientific and technical information generated under a NASA contract or grant and considered an important contribution to existing knowledge.

TECHNICAL TRANSLATIONS: Information published in a foreign language considered to merit NASA distribution in English.

SPECIAL PUBLICATIONS: Information derived from or of value to NASA activities. Publications include final reports of major projects, monographs, data compilations, handbooks, sourcebooks, and special bibliographies.

TECHNOLOGY UTILIZATION PUBLICATIONS: Information on technology used by NASA that may be of particular interest in commercial and other non-aerospace applications. Publications include Tech Briefs, Technology Utilization Reports and Technology Surveys.

Details on the availability of these publications may be obtained from:

SCIENTIFIC AND TECHNICAL INFORMATION OFFICE

NATIONAL AERONAUTICS AND SPACE ADMINISTRATION

Washington, D.C. 20546